Dynamic Model and Security Assessment of Highly Electrified Industrial Hubs With Power-To-X Assets

Numerical simulation-based analysis

Diego Irazoqui Ahlig

Delft University of Technology

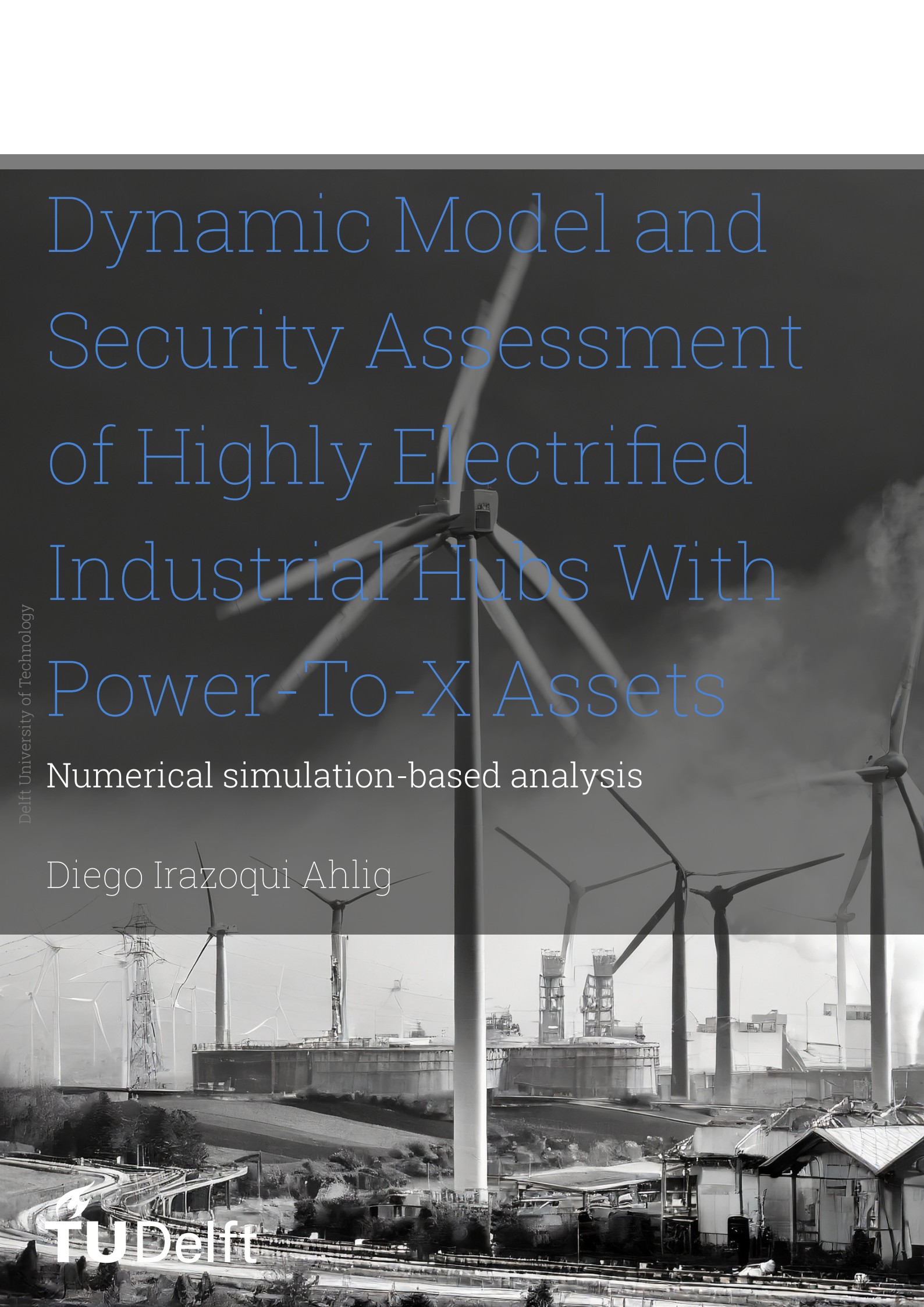

TU Delft

Dynamic Model and Security Assessment of Highly Electrified Industrial Hubs With Power-To-X Assets

Numerical simulation-based analysis

by

Diego Irazoqui Ahlig

to obtain the degree of Master of Science

at the Delft University of Technology,

to be defended publicly on Wednesday May 29th, 2024 at 10:00 AM.

Student number:	5838282	
Project duration:	August 1st, 2023 - May 10th, 2024	
Thesis committee:	Prof. dr. ir. J.L. Rueda Torres,	TU Delft, supervisor
	Dr. ir. Jianning Dong,	TU Delft
	Dr. Pedro P. Vergara,	TU Delft
	Dr. Digvijay Gusain,	Shell

This thesis is confidential and cannot be made public until May 29, 2026.

Cover:	Image generated using Adobe Firefly from ”electrified industrial site” prompt
Style:	TU Delft Report Style, with modifications by Daan Zwaneveld

An electronic version of this thesis is available at `http://repository.tudelft.nl/`.

TU Delft

Preface

This report was developed by the author as part of the research project titled "*Optimal, Secure, and Modular Development of Multi-energy Networks*" (MADURO). The project is conducted by the Intelligent Electrical Power Grids (IEPG) research group at the Technical University of Delft, specifically by the Dynamic Stability of Sustainable Electrical Power System team led by Prof. Dr. Ir. José Luis Rueda Torres.

The MADURO project is supported by Shell. However, the analysis and results presented in this report reflect the opinions of the author and supervisor independently of the company.

The reader is assumed to have a basic understanding of industrial energy infrastructure. Those particularly interested in the case study can refer to Chapter 3. A decarbonized model of an oil refinery is discussed in Chapter 4, while the simulations and results are presented in Chapter 5. The summary of the research, its conclusions, and future recommendations are provided in Chapter 6.

I thank my daily supervisor, José Luis Rueda Torres, for his advice and feedback throughout this work. I also extend my gratitude to Dr. Digvijay Gusain for hosting me at Shell's offices and for his knowledge and guidance. This journey was challenging yet enjoyable, contributing to the future of decarbonization.

Diego Irazoqui Ahlig
Rotterdam, May 2024

Abstract

Decarbonizing industrial processes by transitioning to carbon-neutral energy sources poses significant challenges for industrial operations. The integration of technologies such as Power-To-Heat (PtH) with electric boilers and furnaces, Power-To-Gas (PtG) facilities employing electrolyzers, variable speed drives for energy-intensive machinery, and the increased use of renewable energy sources like wind and solar power plants are reshaping the grid and industrial landscape. This transformation adds complexity and risks, making it a significant endeavor to address emissions from daily operations while maintaining operational security. The industrial sector is crucial in achieving future greenhouse gas (GHG) emissions reduction targets. In Rotterdam's Pernis-Botlek area, where fossil gas accounts for 55% of the 130 PJ/yr average energy consumption for operational needs, the magnitude of this challenge is evident.

This master's thesis explores the dynamic security of highly electrified industrial hubs integrating Power-To-X conversion facilities through model and simulation-based analysis. The research focuses on developing an industrial site network that integrates individual electric loads while anticipating challenges from the evolving electrical grid. Utilizing DIgSILENT PowerFactory, the study simulates operational scenarios and network disturbances to evaluate the impact of these technological changes. Additionally, the thesis proposes mitigation strategies and operational enhancements to ensure continuous and efficient operations.

The developed model aims to provide a versatile and adaptable representation of industrial sites, drawing on existing literature and reflecting the static and dynamic performance of real power systems within the industrial sector. Through numerical simulations and the analysis of performance metrics, critical issues arising from disturbances are identified and examined to find possible solutions.

Contents

List of Figures

List of Tables

1

Introduction

1.1. Problem Definition

The global effort to mitigate climate change and achieve decarbonization has prompted stringent regulations and policies to reduce greenhouse gas emissions across various sectors. The European Union (EU) has set an ambitious goal of attaining an 80% reduction in greenhouse gas (GHG) emission by 2050, compared to 1990 levels [1]. In the Netherlands, the National Climate Agreement [2], issued by the Dutch government, initially targeted a 49% reduction in national GHG emissions by 2030, relative to 1990 levels. However, this objective was later raised to align with the European Commission's "Fit for 55 Package", which aims to reduce net GHG emissions by at least 55% by 2030 [3] [4].

The industrial sector, which accounts for a significant portion of global energy consumption and carbon dioxide (CO_2) emissions, faces immense challenges in transitioning towards a sustainable and low-carbon future. According to the International Energy Agency (IEA), the industrial sector is responsible for approximately 37% of global energy consumption and 24% of direct CO_2 emissions from fuel combustion [5]. In the Netherlands, the industry accounted for around 31% of the country's total GHG emissions in 2021 [4]. These figures underscore the urgency and importance of decarbonizing industrial processes and operations to meet National and European goals.

Nevertheless, reducing emissions in the industrial sector requires a significant technological transition related to the energy supply and industrial process technology. On the grid side, introducing intermittent renewable energy sources, such as wind and solar power, and the increasing adoption of power converter-interfaced technologies leads to challenges in maintaining a stable and reliable power

supply [6]. Behind the fence of the industrial sites, various decarbonization strategies are being explored, including integrating Power-to-X (PtX) technologies and electrifying energy-intensive processes (i.e., electric boilers or large variable speed interfaced electrical machines).

To effectively navigate this technological transition and achieve decarbonization targets, it is crucial to develop comprehensive models that can accurately assess the dynamic electrical behavior of these emerging carbon-neutral sites. Current analyses often focus on individual technologies, failing to capture the intricate dynamics and interactions between various components within the industrial electrical ecosystem. The interdependencies between renewable energy sources, energy storage systems, PtX conversion facilities, and industrial energy demand profiles result in complex non-linear dynamic phenomena that should be adequately represented through state-of-the-art modeling tools.

A generic and integrated model of the industrial electrical network is required to holistically assess the overall system's dynamic behavior under this completely new technological landscape. Such a model should encompass the time-varying nature of renewable energy sources, power electronic converters' dynamic characteristics, and the industrial loads' transient responses. The model is expected to provide valuable insights into the overall system's stability during various operating conditions and disturbances by capturing the device and system-wide dynamic response. This knowledge is crucial to informed decision-making and strategic planning to ensure the successful implementation and operation of decarbonization initiatives in the industrial sector.

1.2. Report Outline

The report begins with an introductory chapter (Chapter 1), setting the stage for the study by defining the problem. Additionally, this section discusses the research objectives and questions, the methodology employed, and the contributions made by the study. In Chapter 2, the state-of-the-art is depicted by a thorough bibliographic review. Chapter 3 defines the specific case study of an oil refinery in the Pernis-Botlek area, highlighting the challenges in upgrading the industrial electrical system and detailing the key modeling and simulation assumptions.

Chapter 4 describes the proposed generic model of the industrial energy hub. This chapter outlines the chosen network topology and the dynamic models for the industrial loads. It also explores various scenarios that were analyzed. Chapter 5 presents an analysis of the numerical simulations conducted, detailing the methodological approaches used and summarizing the findings for each scenario investigated. Finally, the report concludes with Chapter 6, which recaps the project scope and methodological approach, highlights the most significant findings, discusses the contributions made, and suggests future research topics in this domain.

1.3. Objective and Research Questions

The objective of this work is ***to develop a generic model of an industrial electrical network with Power-to-X processes and evaluate mitigation strategies to enable continuity of operations during external and internal network disturbances***. This entails in-depth network modeling, encompassing industrial load components, including their corresponding controllers, and introducing electrical disturbances. DIgSILENT PowerFactory is used to create the model and perform RMS simulations, followed by a quantitative and qualitative result analysis.

The objective is addressed through the following research questions:

- What is a suitable generic topology for a digital model of an industrial hub to investigate its stability performance and interaction with an HV network under critical disturbances?
- What is a proper modeling depth to simulate steady-state and dynamic responses of an industrial hub?
- How to effectively manage the controllable assets of the industrial hub to ensure resiliency to both local and external disturbances?

1.4. Research Methodology

The initial phase of the research involved an extensive literature review focusing on the modeling of electrical industrial loads. This encompassed developing static and dynamic models for voltage and frequency dependencies. These models serve as the foundation for creating a universal industrial site network, which can be customized to depict various industrial processes or locations. Subsequently, this model is tailored to represent Shell's decarbonized oil refinery in the Port of Rotterdam and is integrated into a representative grid model of an industrial region, such as Pernis-Botlek in Rotterdam.

Following this, a literature review on external grid characterization and historical grid events was conducted to pinpoint potentially hazardous power system conditions that could disrupt the operation of electrified industries. The performance of the industrial load under various power system conditions is evaluated by introducing critical events and scenarios categorized as low-probability yet high-impact occurrences. Based on this evaluation, strategies will be recommended to safeguard operational continuity. These models and protective measures will be implemented using simulation tools like DIgSILENT PowerFactory.

The research approach methodology is depicted in Figure 1.1. Notably, the development of the industrial network model and the comprehensive integration of all components within the PowerFactory model are emphasized, representing key achievements during the thesis work. The absence of a benchmark industrial network topology in existing literature, as well as a singular network model

encompassing the broad array of electrical components found within an industrial site, was identified and developed during this study.

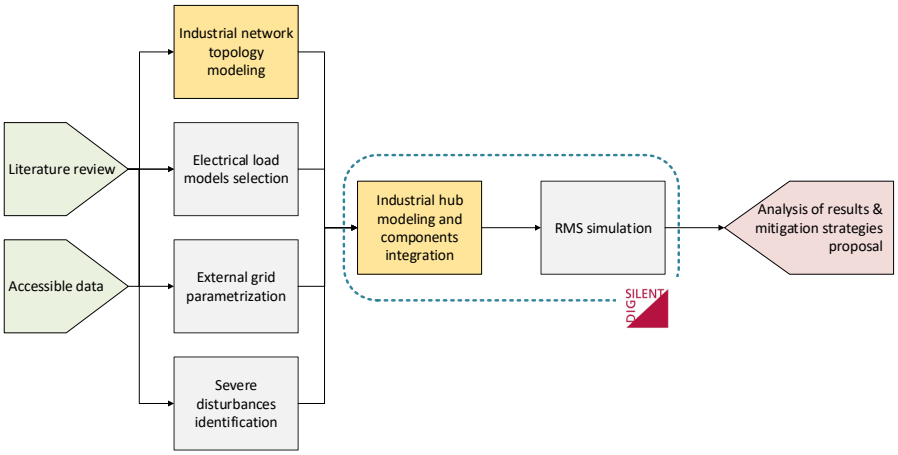

Figure 1.1: Research methodology workflow

1.5. Contributions

This thesis presents three distinct contributions. Firstly, a generic industrial electrical network topology has been developed to integrate the different electrified loads into one interrelated system. A representative industrial load mix has been implemented from a literature review of individual components. The model can be tailored for studies such as reliability assessments or cost optimization of industrial operations subjected to energy supply variability. This thesis demonstrates an application case related to contingency analysis based on RMS simulation.

Secondly, a characterization of the external grid was proposed to represent the transformation due to the introduction of inverter-based technologies, such as wind and solar power plants. This characterization enables the simulation of the external grid over time, facilitating the analysis of the gradual integration of distributed renewable energy sources or the representation of different locations. A description of the impact of these technological changes is provided, including reduced inertia, low short-circuit levels, and a decrease in frequency reserves in the bulk system.

Lastly, severe contingencies were identified, and mitigation measures were proposed, implemented, and analyzed for their effectiveness. These measures include operating the electrolyzer as a primary frequency reserve based on active power-frequency droop characteristics, implementing synchronous condensers and flywheels to improve reactive power injection for voltage control and enhance inertial response, and reviewing new protection configurations for industrial assets, prioritizing critical loads to ensure the continuity of operations.

2

Literature Review

Industrial sites have long been integrated with the grid to power essential machinery like pumps, fans, and compressors. A typical network topology for industrial sites, illustrated in Figure 2.1 sourced from [7], involves an external grid connection at the Point of Common Coupling (PCC) on the High Voltage (HV) level - typically 63 kV - and an internal Medium Voltage (MV) distribution level at 20 kV. Aggregated low voltage (LV) loads are also linked at a lower MV level, around 5.5 kV. At the MV distribution level, redundant synchronous generators (SGs) are connected through their respective step-up transformers, outlining the network's structural design. Internal MV busbars and substations are strategically placed and interconnected to facilitate electricity distribution throughout the industrial site. Variations in network configurations may occur based on the presence of SGs, the characteristics of loads, and the specific industrial processes in operation.

Various network topologies are also detailed in existing literature, such as [8], which presents different MV distribution network structures, [9] showcasing a typical single-line diagram of an oil refinery, and [10] elaborating on grid layouts within port areas. Furthermore, benchmark networks like those enumerated in [11], such as CIGRE or IEEE test networks, aim to serve as generic representations of transmission and distribution grids, adaptable in size and ratings for diverse stability assessments, congestion management, and reliability analyses.

While disclosing actual industrial network topologies can be restricted due to confidentiality concerns, examples are available for review in publications like [12], depicting an oil refinery network in Mexico, [13] showcasing a 200 MW oil refinery unit in Iran, and [14] which features a detailed model

created in Dig-SILENT PowerFactory, encompassing LV busbars of an existing facility in Delta, Egypt. Experts consulted from the Pulp and Paper, Food and Beverage, and Oil and Gas sectors have confirmed that the illustrated example in Figure 2.1 represents a branch of a conventional industrial electrical network. Multiple such branches are typically found across a site, tailored to suit its power demands. Local generation facilities like SGs can also differentiate network configurations; while commonly seen in refineries or pulp mills, they may not be prevalent in the Food and Beverage sector due to varying supplementary processes. For instance, in refineries, exhaust gases [15], or in the pulp industry, black liquor [16] can be burnt to generate steam to power thermal generation units.

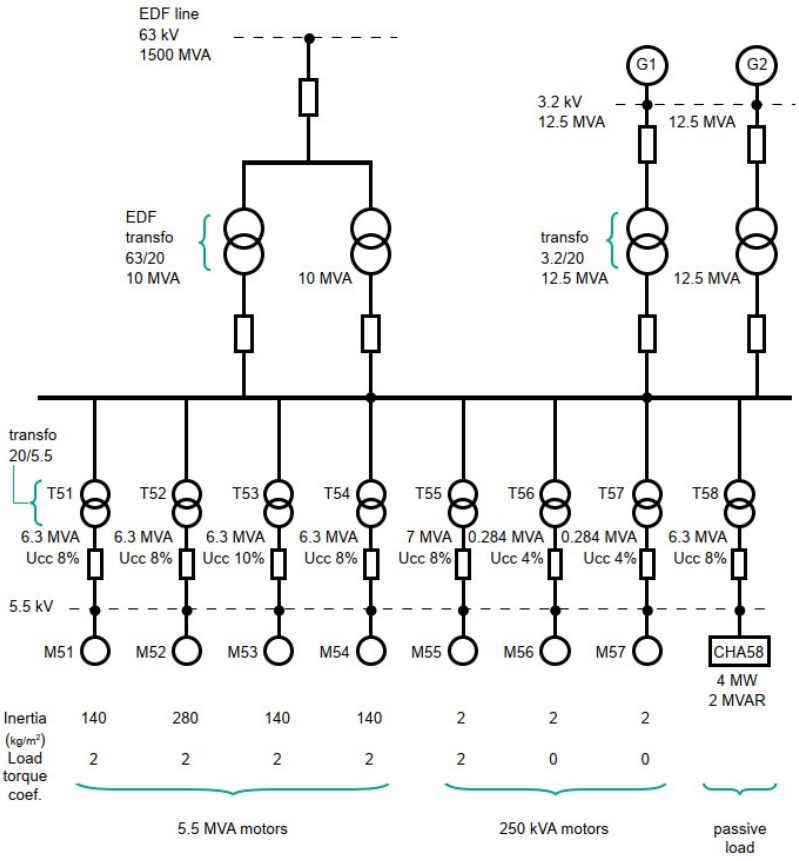

Figure 2.1: Industrial Network Topology (inspired from [7])

The highlighted examples showcase the state-of-the-art industrial electrical power networks operating across various voltage levels, spanning from Low Voltage (LV) - up to 1 kV, Medium Voltage (MV) - 1 kV to 33 kV, to High Voltage (HV) - above 33 kV. The number of busbars can vary based on the system's complexity and redundancy requirements, with the network topology often adapting to these variables across different industrial settings. Referring to IEEE recommended practices for industrial sites [17] and electrical component manufacturer handbooks ([18] [19]), the following network topology features at different voltage levels can be summarized as:

- **HV network**: Typically operates at transmission levels ranging from 60 to 765 kV, serving as the

PCC with the external grid.

- **MV network**: Designed for voltage distribution within the industrial facility, varying from 2.4 kV to 35 kV. A ring configuration is commonly employed to enhance redundancy and reliability, enabling power rerouting during faults or maintenance to minimize interruptions.
- **LV network**: Radial topology is preferred, operating between 120 and 725 V, for its cost-effectiveness. In scenarios requiring increased reliability, a ring configuration or emergency power supply solutions, such as diesel generators, can be strategically placed to power critical loads during emergencies.

While the aforementioned examples primarily focused on SGs, most frequently consisting of thermal units like steam turbines or combined heat and power (CHP) plants, literature addressing the integration of distributed renewable energy sources (DRES) in industrial network planning and design remains scarce. Available research is done at the grid level as in [20] focusing on the ICT reliability of DRES integration; [21] that focuses on the multi-energy system. In Australia, the local energy market operator (AEMO) aggregates load demand, including industrial load, to evaluate the integration of photovoltaic panels (PVs) [22]. In [23], the industrial load is further desegregated into four induction machines depending on the driven mechanical load and directly connected to an IEEE test system for voltage stability analysis. In addition to desegregating the load, distributed energy sources are included in such a study.

Other cases simply connect individual assets to benchmark transmission grids without further analysis on the integration of DRES. [24] recreates the dynamics of multiple induction motors and assesses the dynamic frequency response while introducing the aggregated model to the IEEE 9-bus benchmark network. Other studies on electric boilers [25] connected to an LV grid or electrolyzer [26] [27] connected to the Dutch 220 kV transmission level follow the same approach. [28] explores the integration of variable speed drives (VSDs) and uses the two-area, four-generator network available in [29]. None of these cases approach to model the electricity network of an industrial site, including the electrification of several assets into a single integrated model.

It is conceivable that the criteria to integrate DRES into the industrial network will aim to minimize capital expenditure (CAPEX) for substation equipment while reducing transmission losses, which will heavily influence new architectural decisions. For illustrative purposes, the integration of renewable energy at industrial hubs, exemplified by the port of Rotterdam, can be articulated through two prevalent approaches outlined by TenneT's available data sources ([30] [31]). Renewable energy sourced from wind or solar installations may be harnessed and channeled through two-winding step-up transformers for transmission at HV levels to industrial sites, exemplified by the solar power plant in Ooltgensplaat or wind power projects in Maasvlakte 2 or Hellegatsplein. Alternatively, integration via three-winding transformers allows one winding to link with the renewable energy source at MV or HV levels, with a

second HV winding connecting to the PCC alongside the grid. The third winding is tied to MV busbars that likely interface with the industrial site. Symbolic of this configuration, the Haliade-X [32] 12 MW wind turbine transmits energy via 66 kV lines, directing power flow directly to the Maasvlakte industrial hub at 25 kV or linking to the HV grid at a 150 kV busbar. Correspondingly, Scaldia's 54.5 MWp solar facility [33] can supply the Borssele 10 kV busbar or the 150 kV transmission level. These sites are integrated within the Botlek 150 kV grid frameworks specified in [34], aligning with TenneT datasets accessible through ArcGIS [31].

On the load side, individual asset models are readily available, where [35] aggregates six induction machines for comparative analysis against actual datasets; institutions like the Western Electricity Coordinating Council (WECC) created composite models like the one detailed in [36]. There are examples showcasing the representation of a VSD driving a 200 kW rotating machine in PowerFactory [37], simulating internal VSD components like the rectifier, DC bus, output inverter, and controller framework. As previously cited, [28] delves deeper into enhancing dynamic VSD models for electromagnetic transient (EMT) analyses. While electric boilers, electrolyzers, and EMT phenomena in AC Arc Furnaces are addressed, as seen in [26], [27], [25], [38], and [39]. **It should be noted that there is a gap regarding individual component modeling and grid integration, whereby no dedicated network topology encompasses various industrial components coexisting on-site within a unified model interconnected to an external transmission grid representation.**

The transition towards renewable energy sources and the increasing electrification of industrial assets is reshaping the dynamics of electrical power systems at industrial sites. Traditional fossil fuel-based generators are replaced with intermittent sources, and as energy-intensive processes undergo electrification, these facilities' load and power flow profiles are undergoing profound changes. These transformations necessitate a comprehensive study of the new electrical power dynamics to ensure the industrial site's reliable, efficient, and cost-effective operation. Thorough analysis and simulations are required to optimize these evolving electrical networks' design, control strategies, and protection systems, ensuring seamless integration of new-fashioned technologies. The reduction of total system inertia (TSI) and the increase in Rate of Change of Frequency (RoCoF) were identified by the European Network of Transmission System Operators for Electricity (ENTSO-E) as the top power system stability challenges. The complete list of the identified stability issues can be found in Table 2.1 (retrieved from [40]).

Table 2.1: ENTSO identified top 11 issues (retrieved from [40])

Ranking	Score	Issue
1	17.35	Decrease of inertia
2	10.16	Resonances due to cables and Power electronics
3	9.84	Reduction of transient stability margins
4	8.91	Missing or wrong participation of PE-connected generators and loads in frequency containment
5	8.19	PE Controller interaction with each other and passive AC components
6	7.50	Loss of devices in the context of fault-ride-through capability
7	7.00	Lack of reactive power
8	6.91	Introduction of new power oscillations and/or reduced damping of existing power oscillations
9	6.09	Excess of reactive power
10	4.27	Voltage Dip-Induced Frequency Dip
11	3.87	Altered static and dynamic voltage dependence of loads

Numerous reports and studies by Transmission System Operators (TSOs) in Europe delve deep into critical aspects such as the reduction of inertia and short-circuit levels, detailed in publications like [41], [42], and [43]. Similarly, AEMO has published technical reports addressing future power system risks, accessible through citations like [44]. A special focus has been placed on grid splitting, as addressed by AEMO in [45]. Recommendations were made for contingencies that were not considered possible before but are becoming likely possible due to climate change and the new technological landscape.

The North American Electric Reliability Corporation (NERC) contributes findings on short-circuit levels in their report [46]. In contrast, discussions on system scarcities are further explored in literature like [47]. Addressing the reduction of inertia attributed to renewables penetration, studies such as [48], [49], and [50] offer significant insights into the field. Furthermore, the adequacy of primary frequency response in future scenarios is closely examined in works like [51].

In summary, while there is established knowledge of industrial electric network modeling, there is an increasing need to integrate DRES and electrified loads into a single network. Extensive research on individual component modeling exists, yet an integrated approach to system-wide electrical network modeling is lacking. Seamless integration of components into a unified network model to evaluate dynamic behaviors is pivotal in the ongoing energy transition. The shift towards inverter-based resources (IBRs) from solar or wind power plants necessitates a thorough reevaluation of grid technicalities, emphasizing the importance of adapting to these dynamic changes. TSOs and key stakeholders focus on identifying future challenges and disturbances while analyzing mitigation strategies to uphold the system's resilience and reliability in the evolving energy landscape.

3

Case of Study Definition: Oil Refinery in the Pernis-Botlek area

The industrial sector is the second source of CO_$text2$ direct emissions, accounting for 25% of total energy system emissions [5]. If indirect emissions from the electricity and heat generation are included, the number increases to roughly 45%. Therefore, decarbonizing industrial processes through electrification or adopting alternative carbon-neutral fuel production is paramount to achieving decarbonization goals. Nevertheless, the technological shift presents significant challenges for industrial sites. These challenges stem from integrating technologies like PtH or PtG facilities, variable speed drives for energy-intensive equipment, electrical furnaces, and distributed energy resources like wind and solar power plants. Additionally, DRES are being introduced to ensure a clean energy supply, all within the same industrial setting. This shift towards higher dependence on electricity necessitates a closer examination of the technical changes in the electrical power system due to the ongoing energy transition.

This chapter will begin by discussing the electrification of the industrial sector, followed by an exploration of three critical challenges faced by the transmission grid. These challenges include the reduction in total system inertia (TSI), a decrease in short-circuit levels, and the implications of decreasing balancing reserves.

3.1. Challenges Due To Technological Upgrade of the Industrial Electrical System

3.1.1. Electrification

In the 2050 Net Zero Emissions scenario by the International Energy Agency (IEA), electrification and carbon capture, utilization, and storage (CCUS) are projected to contribute significantly to emissions reductions. Energy and material usage efficiency will further enhance this impact. Nearly half of the energy sector's fuel consumption can potentially be replaced with electricity, especially in processes requiring high temperatures up to 1000°C. However, the primary challenge for electrification lies in its economic viability, which depends on electricity costs compared to conventional fuel equipment, as detailed in reports like the one by McKinsey [52].

Focusing on the Dutch industrial forecast, the industry is poised to lead in achieving the 2030 greenhouse gas emissions reduction goals. The Dutch refinery sector accounted for 10 million tonnes of CO_2 emissions between 2016 and 2019. The sector's significant energy consumption, primarily sourced from fossil fuels in gas-fired furnaces and hydrogen production, underscores the urgent need for solutions that reduce carbon-based technology reliance. Strategies such as direct electrification of assets, decarbonized energy carrier substitutions, and direct carbon capture, utilization, and storage (CCUS) are pivotal to achieving this shift.

Regarding the assets likely to be electrified, [5] and [52] mentioned at a high level some processes to be decarbonized through electrification. In [53], a thorough analysis of the Pernis-Botlek area is described. Furthermore, [54] and [15] dive deeper into the options for the chemical sector and the refinery sector, respectively. These reports outline that gas-fired furnaces and steam generation are responsible for a large portion of industrial CO_2 emissions and must be updated. Technological difficulties are being faced for the former, as mentioned in [53]. The high heating requirements make the application of biomass together with carbon capture technologies a more feasible solution economically and technology-wise. Electrical boilers are a more mature technology that uses electrode or resistance heating elements. In any case, efficiency is already around 99%, providing steam up to 350°C, and capacities reaching up to 100 MW [15].

Moreover, shaft equipment currently driven by mechanical drives (i.e., gas or steam turbines), such as large compressors, will likely be the first to be electrified [15][54]. This includes the introduction of variable speed drives (VSD) for electrical motors ranging from 5 MW to replace steam turbines in some processes [53], up to around 40 MW, according to consulted experts in the refinery sector. This approach improves the GHG emissions of such assets and the efficiency and maintenance requirements, as discussed in [9]. These new electric-driven machines will join the already mature induction machine-driven equipment, widely spread across the industry, accounting for 50% to 70% of the electricity demand in some industrial sites [55].

Aside from existing processes being retrofitted to use electricity as an energy carrier, introducing water electrolysis for hydrogen production has become a top trend in the industrial sector. Hydrogen is already present in the industry as a feedstock and reducing agent [56], but less than 1% comes from low-emission technologies. In particular, hydrogen produced through water electrolysis accounts for around 0.1% of global production. To enhance the production of energy carriers from renewable energy resources, the Fit-for-55 package [3] sets a 40 GW electrolyzer installed capacity for 2030. Consequently, the massive introduction of electrolyzers at industrial sites and DRES will reshape the demand for electricity at such sites. For example, in Pernis-Botlek alone, the 2050 scenario forecasts that the Port of Rotterdam will handle up to 30 times the current hydrogen production at the site [53].

To recap, decarbonizing the industrial sector implies a massive electrification of the production processes. Even when zero-carbon energy carriers substitute fossil fuels, these can be produced through electricity-based technologies such as electrolyzers. Consequently, the electrical demand will increase over time, accompanied by a massive introduction of DRES (4 MW for refinery sector electrification alone [15]). The higher dependence on the power system requires a closer look at its technical features to anticipate possible problems and mitigate their effects. The following sections address these major changes in the electrical power system.

3.1.2. Decreasing Total System Inertia and Balancing Reserves

The inertia of an electrical power system refers to the stored kinetic energy in the rotating masses of synchronous generators connected to the system. Mathematically, it is described by Equation 3.1:

$$E_{kinetic} = \frac{1}{2} J \cdot \Omega^2 \tag{3.1}$$

Where:

- E_{kin} is the rotating mass kinetic energy
- J is the moment of inertia in kgm^2
- Ω is the mean angular speed at which the mass is rotating

In traditional power systems, a simpler quantity to describe the system's equivalent inertia is using the inertia constant H measured in seconds [41] [29]. The variable is the ratio between the total kinetic energy stored in the rotating masses of the power system and the rated power S (in MVA) of the synchronous machines.

$$H = \frac{E_{kinetic}}{S} \quad [s] \tag{3.2}$$

Consequently, a higher value of H indicates a higher system inertia and a greater ability to withstand disturbances without significant frequency deviations. The stored kinetic energy acts as a so-called inertial response against sudden changes in the balance between generation and load, stabilizing the system frequency. Traditional hydraulic or thermal units can have a constant of inertia H of around 2 to 4 seconds for the first one and 4 to 10 seconds for the latter. In the case of power converter-interfaced units, this parameter becomes almost zero, even for wind turbines. The electricity generated by the rotating machine is converted to DC and further converted to AC to feed into the grid. Therefore, the inherent inertia of the rotor and blades is decoupled from the grid. [40] shows a future 2030 scenario with an estimation of the inertia constant in different areas of Europe as shown in Figure 3.2. Such a constant will tend to decrease to almost zero in case of the decommissioning of all the SGs of the network, with TSO considering that H falling below 2 s is already an issue to be addressed.

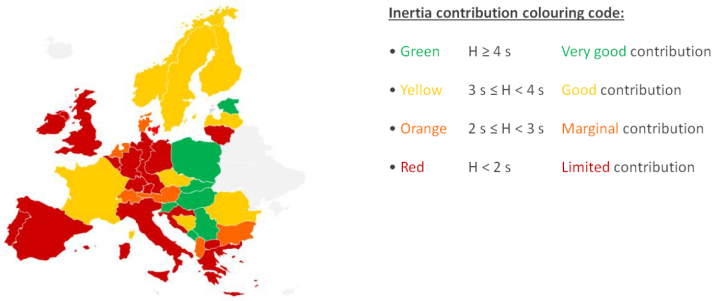

Figure 3.1: Inertia constant across Europe (retrieved from [40])

ENTSO-E conducted a more in-depth study about future challenges [43]. It analyzed the future dynamic challenges of the system due to the energy transition for different scenarios. In particular, the *National Trends (NT)* scenario forecasts the long-term technical conditions according to the current national energy and climate policies of the European countries [57]. One of the most noticeable results is related to the inertia constant for different countries. It represents the number of hours the system inertia is at a certain value. The thicker the violin is, the more hours are at that inertia value. In the case of The Netherlands, this will likely be as low as 1 second by 2030 and decrease to around 0.5 seconds for most of the time in 2040.

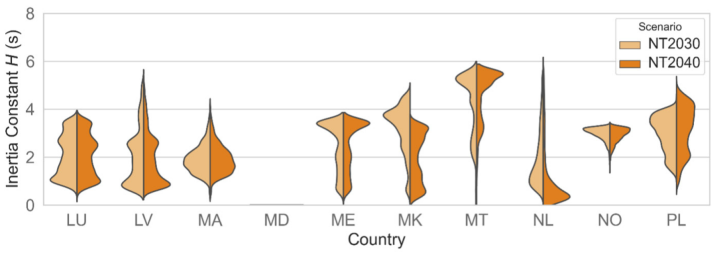

Figure 3.2: Violin plots for NT2030 and 2040 scenarios (retrieved from [43]

The effect of low inertia values is one of the key factors affecting the rate of change of frequency (ROCOF) after a power imbalance. It is described by Equation 3.3. This is a metric that helps to measure the available time that balancing reserves have to kick in. Higher values of ROCOF can be as critical as leading to load-shedding (i.e., disconnection of loads) or even blackout events. In addition to the lower time frame to act, the availability of frequency reserves is also a challenge under sudden power imbalance. Moving from controllable generating units to variable and uncertain DRES decreases the available reserves that can be deployed to withstand the transients after a disturbance.

$$\frac{df}{dt} = ROCOF = \frac{\Delta P_{\text{imbalance}}}{P_{\text{System}}} \cdot \frac{f_0}{2 \cdot H} \quad [\text{Hz/s}] \tag{3.3}$$

3.1.3. Reduced Short-circuit Power

The short-circuit power (S_{cc} in MVA) or current (I_{cc} in kA) is a crucial parameter in assessing the stability and safety of an electrical system. It represents the maximum electric power (or current) flowing through a system point during a short circuit event. It is usually specified at the PCC between the load and the external grid [58]. This value is essential for designing appropriate protection systems, such as circuit breakers and fuses, which must be capable of interrupting these potential high power flows to prevent equipment damage and ensure operational safety. The grid's impedance and active load contribution during the event influence the short-circuit power. A higher short-circuit power indicates a stiffer grid (lower impedance), suggesting that the system can handle larger loads and disturbances with less impact on system voltage and stability. Conversely, a lower short-circuit power implies a weaker grid, which can be more susceptible to voltage dips and fluctuations during large loads or faults. Accurately calculating the short-circuit power at the PCC is vital for grid planning and reliability assessments.

On traditional power systems, SGs contribute to the short-circuit during faults. At the time of a fault, the synchronous machine will act as a current source[46], delivering transient currents as high as 5 to 10 times the nominal current of the machine [59]. Similarly to SGs, induction machines also contribute to the short-circuit current. Consequently, a high or low circuit current depends on the corresponding location within the grid.

IBRs have a completely different behavior. Therefore, a different metric called short-circuit ratio (SCR) is introduced[46]. In the same fashion as short-circuit power, it helps measure the voltage stiffness of the system. A higher SCR implies lower voltage deviation during disturbances in the system. It is defined by the ratio between the short-circuit capacity of the network (S_{cc}) before the connection of the new inverter-based generation source and the rated power of the new source (P_{IBR}), as depicted by Equation 3.4

$$SCR = \frac{S_{cc}}{P_{IBR}}[-] \tag{3.4}$$

The risk of low SCR and short-circuit currents can be summarized in two. Firstly, circuit breakers and protection relays cannot identify and clear the fault (i.e., isolate the damaged circuit from the energy sources) in time to avoid further disturbances in the system. While the high short circuit prevents the voltage of the system from dropping. Secondly, lower fault current contribution results in deeper voltage dips, increasing the risk of load shedding or large blackouts. While IBRs are introduced into the system, both metrics evolve similarly. S_{cc} is used in traditional electrical planning for load sites, while SCR is used in connection studies for non-synchronous generation power plants [46]. It should be mentioned that there is no standard for calculating the SCR index on a weak system (i.e., low or no short-circuit power). Values of SCR above 3 are usually related to a strong grid, while the value falling below 2 represents a weak grid.

3.1.4. Load Shedding

The main objective of the electrical power system is to meet the load demand for active and reactive power at every instant of time [29]. In addition, such supply should meet minimum quality standards such as constant frequency, constant voltage, and a certain reliability level. When those objectives are unmet, remedial actions should be implemented to restore the system's secure and normal operation levels. Unpredictable contingencies such as component outages, faults, and lack of generating capacity, among other contingencies, can be the root cause of the imbalance between generation and demand. The introduction of solar and wind-based generation facilities exacerbates the unpredictability of generating capacity, which threatens the system's stability. Aiming to restore the balance, automatic load shedding on low frequency can be implemented.

Cycling back to the ROCOF definition, Equation 3.5 depicts the impact of a sudden imbalance between generation and demand, which results in a system frequency increasing or decreasing rate. If there is more generation than demand, the frequency will tend to increase, while if there is a lack of generation, the effect will be the opposite. Consequently, if increasing electricity production is impossible, implementing a load-shedding strategy can be a remedial solution to limit the fault effect.

$$\text{ROCOF} = \frac{\Delta P_{\text{imbalance}}}{P_{\text{System}}} \cdot \frac{f_0}{2 \cdot H} \quad \text{[Hz/s]} \tag{3.5}$$

Where:

- $\Delta P_{\text{imbalance}}$ is the power imbalance between generation and demand in W
- P_{Load} is the total total system's load at the instant of the contingency in W
- f_0 is the nominal rated frequency (i.e., 50 or 60 Hz)
- H is the total system inertia (in s)

To further help the understanding of the impact of a power imbalance, an indicator can be introduced as in [60]. The imbalance percentage can be obtained by comparing the actual load and generation after a disturbance as shown in Equation 3.6. If the load exceeds the generation, there is more demand than supply, and the frequency will decrease. The higher such percentage is, the higher the ROCOF will be (in absolute values), and the faster the frequency will decrease.

$$\text{Imbalance Index} = \frac{P_{\text{Load}} - P_{\text{Generation}}}{P_{\text{Generation}}} \cdot 100 \quad [\%] \tag{3.6}$$

Within the research scope of this report, load shedding will be used to prioritize loads that should remain connected to enhance the continuity of operation. Those non-critical loads whose disconnection represents lower or no risk for continuity of operation will be represented to have a more sensitive under-frequency trip. The overall objective is to, ideally, not disconnect any load or just the necessary amount to keep the system stable. The effect of this strategy is depicted in Figure 3.3.

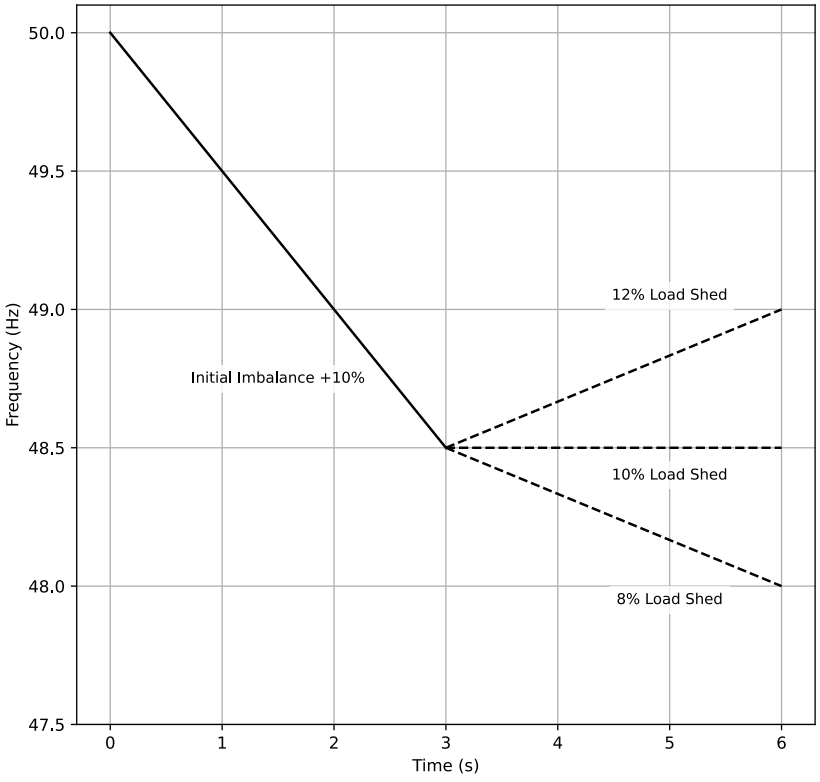

Figure 3.3: Load shedding impact for frequency balancing (reconstructed from [60])

3.2. Zero-emission Shell's Pernis Refinery Modelling

Oil and gas operations account for around 15% of greenhouse gas emissions related to energy utilization, reaching around 5.1 billion tonnes [61]. Reducing the carbon footprint of refineries, a traditional energy-intensive and fossil-fuel-based industry, plays a key role in the transition towards a sustainable and low-carbon future. Within the analyzed future scenarios by the IEA, the emissions intensity will be halved by 2050. Consequently, achieving such optimistic scenarios requires exploring innovative technologies and strategies for decarbonization while maintaining the reliability and continuity of operations of the industrial sites.

In the Netherlands, the Pernis-Botlek area in Rotterdam is one of the largest fuel clusters worldwide. The future outlook for such an area includes a massive introduction of offshore wind power plants, increased green hydrogen production, and the introduction of synthetic fuels and bio-fuels to replace fossil-based products [53]. In this context, electrification plays a significant role in reducing emissions from thermal processes such as steam production (so-called Power-To-Heat), the substitution of shaft equipment such as steam turbines, and the production of hydrogen through water electrolysis (Power-To-Gas). Consequently, Shell's Pernis refinery is selected as a study case. A detailed explanation of the future electrical load mix is described as follows.

To begin with, the options for decarbonization suggested in [15] were considered to create a 500 MW case of study model representative of an industrial site. The electric technology for each category, namely fuel substitution, fuel as a feedstock substitution, and carbon capture to be adopted, is described as follows. Firstly, fuel substitution is considered. This includes introducing electric shaft equipment to replace current steam turbines that drive large gas compressors. Electrical motors fed by variable-speed drives are used in this application. Each unit is assumed to have a nominal capacity of 30 MW as mentioned in [9]. In addition, electric boilers are assumed for steam production, while green hydrogen as a fuel is intended for all gas-fired equipment, including furnaces. No electric furnaces are considered in the scope of this work, as their Technology Readiness Level (TRL) is still low (TRL 3), and low-carbon gas-fired furnaces seem to be a more promising alternative from the techno-economic point of view [53]. Secondly, fuel used as feedstock is also assumed to be replaced by green hydrogen. Thirdly, induction machines will still drive the balance of plant technologies such as pumps, fans, small compressors, and other mechanical equipment. Finally, carbon capture technology is left out of the scope of the analysis. The current energy consumption is summarized in Table 3.1.

Table 3.1: Current energy demand in Shell's Pernis refinery (retrieved from [15])

Commodity	Demand (PJ/yr)	Share
Fuel gas/natural gas as energy use in processes	31.0	58%
Fuel gas/natural gas for hydrogen production via SMR	4.00	8%
Steam use in processes	15.0	28%
Electricity use in processes	3.00	6%

On the one hand, it should be mentioned that part of the fossil fuels is used as an energy source to produce steam in CHP units, reaching up to 11.4 PJ/yr in Shell's Pernis site [15]. At the same time, the remaining amount can be assumed to be used in high-temperature heating processes. accounting for up to 19.6 PJ/yr. With the introduction of electric boilers, the first will no longer be required, while the latter will be covered by green hydrogen. Using a Low Heating Value (LHV) of 120 MJ/kg gives a required production of 163.000 tonnes annually. Furthermore, the fuel used for hydrogen production through Steam Metane Reforming (SMR) or gasification can be neglected, as it is substituted by hydrogen produced through water electrolysis. Besides its future energy source, the current hydrogen use as a feedstock is also electrified. The current production by SMR or gasification reaches around 153.000 tonnes per year [15]. Finally, the demand for electricity to drive electric machines will remain unchanged.

Table 3.2: Decarbonized energy supply alternatives per current used fuel

Energy carrier	Current end use	Demand & units	Decarbonized alternative
Fuel or natural gas	Steam production in CHP plant	11.4 PJ/yr	Neglected in future scenario
Fuel or natural gas	High-temperature heating processes	19.6 PJ/yr	Substituted by hydrogen
Fuel or natural gas	Hydrogen production (SMR)	4.00 PJ/yr	Neglected in future scenario
Hydrogen (SMR, gasification)	Feedstock	153 kt/yr	Water electrolysis
Steam	Production processes	15.0 PJ/yr	Electric boilers
Electricity	Production processes	3.00 PJ/yr	Unchanged

On the other hand, diving deeper into the new energy demand landscape, the total electricity used in the process is assumed to remain the same, except for adding the new electric drives for large gas compressors and the balance of plant (BOP) required for water electrolysis. For the first, based on the Shell expert's consultation, two 30 MW units are considered, with 8400 running hours per year.

This gives an added electricity demand of 1.8 PJ/yr. For the latter, 12% of the energy demand of water electrolysis processes is considered for Balance-Of-Plant (BOP) purposes. An electricity yield of 58.00 kWh/kg is assumed for hydrogen production. Furthermore, electric boiler efficiency is considered to be 99% [53]. A summary of the electricity demand of the low-carbon refinery model is shown in Table 3.3.

Table 3.3: Modeled energy demand in Shell's Pernis low-carbon refinery

Electrified load	Final energy use [units]	Efficiency / Energy yield	Electricity Demand (TWh/yr)	Share
Electrolyzers for hydrogen as fuel	163 kt/yr	58.0 kWh/kg	8.34	35%
Electrolyzers for hydrogen as feedstock	153 kt/yr	58.0 kWh/kg	7.80	33%
Electric boilers	15.0 PJ/yr	99%	4.22	18%
Other electric loads	-	-	3.53	15%

To conclude, the nominal capacity of the modeled industrial load is set to be 500 MW. 60 MW are fixed to be covered by the large VSDs, while the remaining power capacity (440 MW) is allocated to each load type according to the share indicated in Table 3.3. The number of individual units to cover the electricity demand, as well as the power and voltage ratings, were defined based on expert consultation and available components datasheets. In addition. 8400 running hours are considered for every load for calculation simplicity. Consequently, electrolyzer units are assumed to have a nominal capacity of 150 MW connected to 25 kV busbars. Electric boilers are subdivided into large 15 MW heaters connected to 25 kV busbar, and smaller units for lower temperature process heating are assumed into 5 MW power capacity connected to 6.3 kV busbars. Finally, the electric loads connected to low-voltage busbars (0.4 kV) are grouped into 11 MW aggregated loads. The final load mix, including the number of individual units, voltage ratings, and power factor, is summarized in Table 3.4

Table 3.4: Electric Load Data

Load	Voltage (kV)	P (MW)	Q (MVAr)	S (MVA)	PF	Units
Electrolyzers	25	150.00	37.59	154.6	0.97	2.00
Large E-Heater	25	15.00	0.00	15.00	1.00	3.00
Small E-Heaters	6.3	5.00	0.00	5.00	1.00	6.00
Large VSD	6.3	30.00	5.07	30.43	0.99	2.00
LV electric loads	0.4	11.00	6.82	12.94	0.85	6.00
	Total Apparent Power:			**523**	**MVA**	

4

Proposed Generic Model of Industrial Energy Hub

4.1. Network Topology

As outlined in Chapter 2, there is a noticeable gap between modeling individual loads and their integration into a cohesive network topology for an industrial site. To address this, a generic and adaptable network topology was developed, as shown in Figure 4.1. This layout is designed to be flexible and suitable for various industrial configurations incorporating DRES such as WPP or PV systems. The diagram demonstrates the connections across different voltage levels and components within the electrical power distribution system.

The framework begins with an external grid connection, serving as the primary power source or a backup, depending on the site's power purchase agreement. This connection involves an HV busbar, typically operating above 60kV, linked to the industrial site through a substation known as the point of common coupling (PCC). Additionally, SGs are connected to the MV distribution bus, which transports electricity to various site zones. For the integration of DRES, a three-winding transformer setup allows for versatile connection options, either directly to a nearby MV bus or back to the external grid.

Three principal voltage levels characterize the onsite network topology, apart from the HV level:

- MV Distribution Busbar (15 to 33kV): This busbar distributes power from the HV busbar via step-down transformers and transports it throughout the industrial hub at MV levels. Moreover, it is capable of directly powering significant loads like electrolyzers or large electric boilers.
- MV Busbar (1 to 15kV): Operating at a lower MV range, this busbar primarily serves individual large motors. It is also used to step the voltage down to LV levels.
- LV Busbar (<1kV): This level distributes electrical power to smaller loads or auxiliary systems within the site.

The design incorporates two radial branches at the lower MV level and a direct step-down from the MV distribution level to LV, aiming to represent sites without an intermediate MV level. This topology is versatile, and it can reconfigure circuit breakers in each line to create a mesh (as depicted in Figure 4.1), open loop, or radial setup. Additionally, the system enables the DRES injection point to accommodate sites dedicated to specific zero-carbon processes, such as hydrogen production, that require that the energy supply be directly fed from renewable resources.

In addition, the busbar voltage level diversity can also be modified with little effort. Diverse types of industrial loads can be integrated to carry out studies with different goals. It supports detailed evaluations of both short-term and long-term frequency and voltage stability, reliability, and flexibility of the electrified site, preventing excessive aggregation of electrified industrial loads.

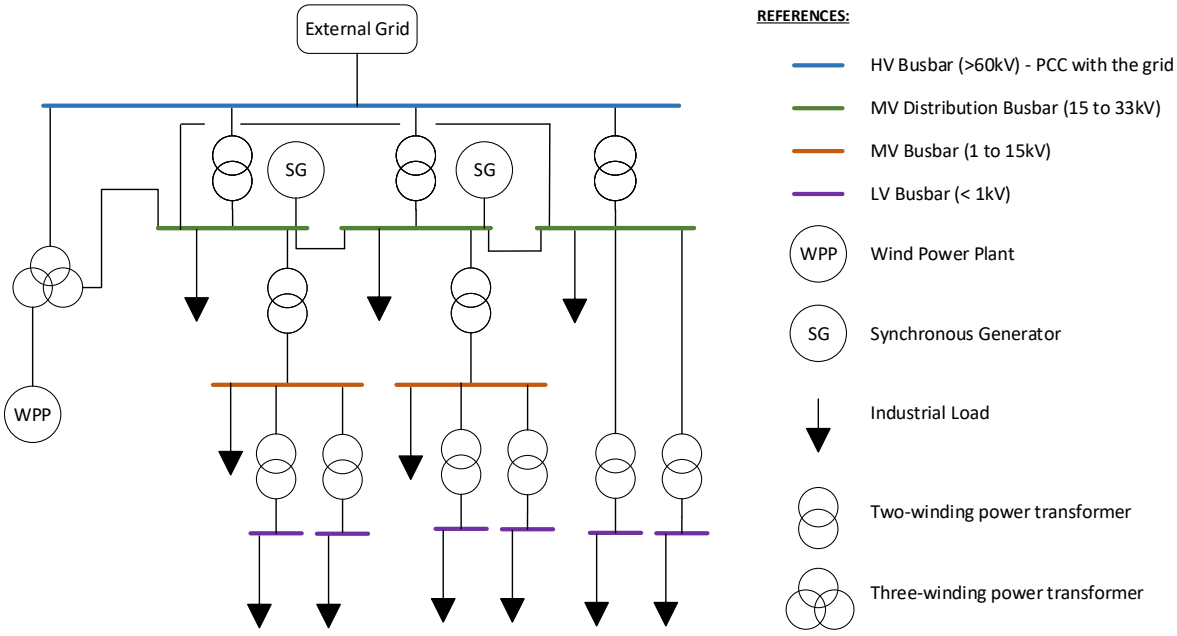

Figure 4.1: Proposed generic network topology

In the context of this thesis, the formulated generic industrial network topology presented in Figure 4.1 is integrated with a 220kV transmission grid, depicted by the benchmark *two area, four generator* (2A4G) network from [29]. To match the PCC voltage level of the industrial site (150 kV) with the external transmission line (220 kV), an ideal two-winding transformer, characterized by an absence of losses and short-circuit impedance, is employed. In the 2A4G network, the original synchronous generators (SGs) have been replaced by two configurable external grids PowerFactory components. The transmission grid setup is detailed in Figure 4.2. Load B represents the aggregated load on the transmission network. For such purpose, the Pernis-Botlek area is considered, where Shell Pernis accounts for 25% ([53]) of the final electricity consumption. This model presumes that all industrial hubs in the Pernis region will mimic the same electrification trend over time, maintaining their current proportion of electricity usage into the future. Therefore, Load B is set to 1500 MVA, that is, 75% of the electricity demand on the proposed model.

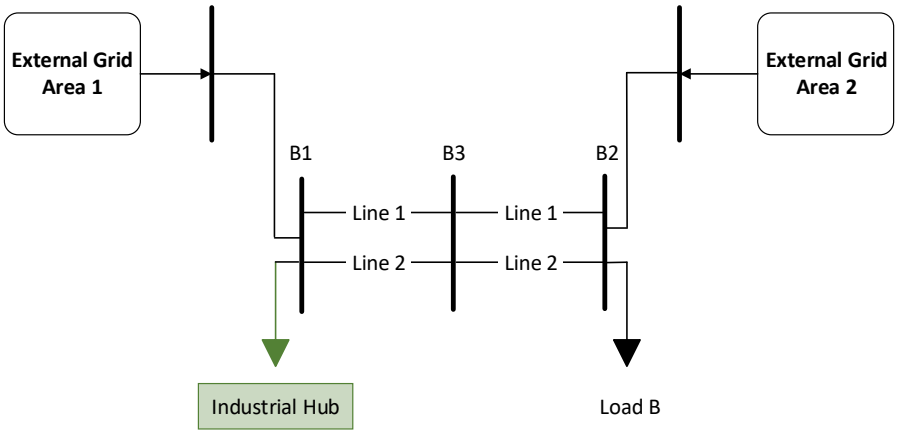

Figure 4.2: Modified two areas, four generators network

4.2. Representation of Loads Dynamics

In the following sections, the selected models to be implemented in the PowerFactory model are discussed, including the most important parameters.

4.2.1. Aggregated Induction Machines

The Western Electricity Coordinating Council (WECC) Composite Load Model (CLM) was developed based on detailed physical models of different loads as well as a measurement-based approach to identify model parameters [62]. The complete model specification can be found in [36].

WECC model is used to represent aggregated load voltage loads. This includes four different motor dynamic behaviors depending on the mechanical load driven by the electrical machine rotor. In addition, electrical load (constant power consumption if the voltage is above a certain threshold) and ZIP constant load (representing other low voltage loads such as lights, offices, etc.). A 5th-order physical model of the induction machine represents the four motors' dynamic behavior. In addition, the mechanical loads driven by each motor type are as follows:

- Motor A: three-phase motor driving a low-inertia and constant torque load (e.g., gas compressors or positive displacement pumps)
- Motor B: three-phase motor driving a high-inertia and variable torque loads (e.g., fans or air handling units)
- Motor C: three-phase motor driving a low-inertia and variable torque load (e.g., centrifugal pumps)
- Motor D: single-phase motor (neglected in the current analysis)

Equal shares of motors A, B, and C are introduced into the aggregated load. Motor D is neglected, as it is usually a low share of the total demand. The most important parameters are the voltage trip settings. As a starting point, the settings listed in Table 4.1 are introduced. The settings are built under IEC 60034-1 limits.

Table 4.1: Induction Machine tripping conditions

Variable Name	Value	Unit	Description
Vtr1	0.92	p.u.	First V trip V
Ttr1	3.5	s	First V trip delay time
Ftr1	1	-	First V trip fraction
Vrc1	0	p.u.	First V reconnection V
Trc1	9999	s	First V reconnection delay time
Vtr2	0.88	p.u.	Second V trip V
Ttr2	0.5	s	Second V trip delay time
Ftr2	1		Second V trip fraction
Vrc2	0	p.u.	Second V reconnection V
Trc2	9999	s	Second V reconnection delay time

The settings are built under IEC 60034-1 criteria showing in Figure 4.3. The standard refers to Area 1, where the machine can provide its primary function without derating. In an induction machine, the primary function is to provide the rated torque (in Nm). Therefore, Area 1 represents the region where the machine operates without derating, while under Area 2, the machine should be able to, but some derating in its torque can be expected. The voltage limits allow a short time window operating under 0.92 pu before tripping for undervoltage. The tripping times are taken from WECC load shedding guidelines [63].

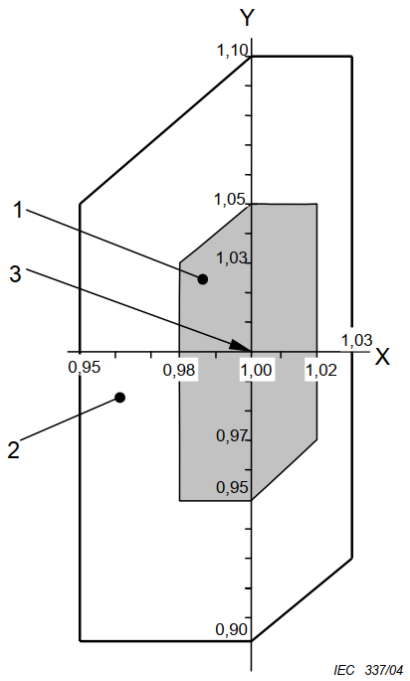

1 zone A
2 zone B (outside zone A)
3 rating point

Figure 4.3: IEC 60064 Voltage (X-axis) and frequency (Y-axis) operational limits

4.2.2. Low Voltage Static Loads

Static electrical loads are those with constant electricity demand without significant variation over time. Static loads include lighting, heating, ventilation, small air conditioning (HVAC) systems, and auxiliary facilities such as computer servers or office rooms. Unlike dynamic loads, which are highly dependent on the operation and production equipment characteristics, electric dynamics are modeled just by the relation between demanded active and reactive power and the voltage terminal.

For this purpose, the ZIP exponential model is considered within the WECC composite load frame. It represents the voltage and frequency dependency of loads' active and reactive power with the following equation:

$$P = P_0 \left[P_{1c} \cdot \left(\frac{v}{v_0} \right)^{P_{1e}} + P_{2c} \cdot \left(\frac{v}{v_0} \right)^{P_{2e}} + 1 - P_{1c} - P_{2c} \right] \cdot (1 + P_{frq} \cdot \Delta f) \tag{4.1}$$

$$Q = Q_0 \left[Q_{1c} \cdot \left(\frac{v}{v_0} \right)^{Q_{1e}} + Q_{2c} \cdot \left(\frac{v}{v_0} \right)^{Q_{2e}} + 1 - Q_{1c} - Q_{2c} \right] \cdot (1 + Q_{frq} \cdot \Delta f) \tag{4.2}$$

Where P_0 is the nominal active power of the static load, and Q_0 is the reactive power. The power factor PFs is used to calculate the nominal reactive power. In addition, a component representing the frequency dependency is defined by multiplying the ZIP exponential model by a factor that depends on the deviation of the network frequency from the nominal value. Further elaboration on the model can be found in [36] [29], and [62].

The input parameters are left by default because the static load share in the aggregated load model will be considered low (set to be 5% of the aggregated low voltage loads). The other parameter description and values are listed in Table 4.2

Table 4.2: Summary of key parameters

Variable Name	Value	Unit	Description
PFs	0.99	-	Power factor
P_{1e}	2	-	P1 exponent
P_{1c}	0.3	-	P1 coefficient
P_{2e}	1	-	P2 exponent
P_{2c}	0.7	-	P2 coefficient
P_{frq}	0	-	P frequency sensitivity
Q_{1e}	2	-	Q1 exponent
Q_{1c}	-0.5	-	Q1 coefficient
Q_{2e}	1	-	Q2 exponent
Q_{2c}	1.5	-	Q2 coefficient
Q_{frq}	-1	-	Q frequency sensitivity

4.2.3. Low Voltage Electronic Loads

In the scope of this research, WECC electronic load is used to represent the aggregation of low-voltage variable speed drives (VSDs). A more thorough description of VSDs can be found in subsection 4.2.6. The behavior of the WECC electronic load model can be summarized as indicated below. The parametrization implemented in PowerFactory is indicated in Table 4.3

- If the terminal voltage V_t of the load is higher than the threshold indicated by V_{d1}, the active and reactive power of the load are kept constant.
- If V_t is lower than the tripping threshold V_{d2}, the load is disconnected from the supply.
- If the terminal voltage is between V_{d1} and V_{d2}, the power consumption is decreased linearly.

Table 4.3: WECC Electronic load parametrization

Variable Name	Value	Unit	Description
PFel	1	-	Electronic load power factor
V_{d1}	0.9	p.u.	Voltage below which electronic load decreases
V_{d2}	0.75	p.u.	Voltage below which electronic load is zero
frcel	0	-	Fraction that recovers from low voltage trip

4.2.4. Electrolyzer

The Proton Exchange Membrane (PEM) electrolyzers are modeled following [64]. Details of the hydrogen production technology and process can be found in [65]. Overall, it can be said that the hydrogen production rate is directly related to the DC current flowing through it. An AC/DC converter (i.e., rectifier) is introduced between the electrolyzer stacks and the electricity supply. Therefore, the dynamic behavior of the asset is decoupled on the AC side and can be represented as a ZIP load with constant power under steady-state operation.

Nevertheless, PEM electrolyzers have a unique feature, which is their high ramping rate, which can reach up to 50% of their nominal capacity per second. During cold start, this rate is much lower, but this will be neglected in the scope of the study as it will be assumed to be a steady-state operation before assessing the dynamic response to external and internal disturbances. A droop controller is attached to each electrolyzer to provide frequency containment reserves (FCR) when required. The parameters are summarized in Table 4.4, while the control strategy is illustrated in Figure 4.4.

Table 4.4: Electrolyzer FCR control parametrization

Variable Name	Value	Unit	Description
FCR_{db}	0.2	Hz	FCR deadband
FCR_{bid}	50	MW	FCR bidsize
Δf_{max}	1	Hz	Maximum FCR frequency deviation
P_{ref}	75	MW	Reference active power flow value
f_{ref}	50	Hz	Nominal frequency
grad	80	MW/s	Electrolyser ramp rate
Bid_{min}	-50	MW	Negative bid limit
P_{min}	30	MW	Electrolyser technical minimum active power
Bid_{max}	100	MW	Positive bid limit
P_{max}	125	MW	Electrolyser active power rating

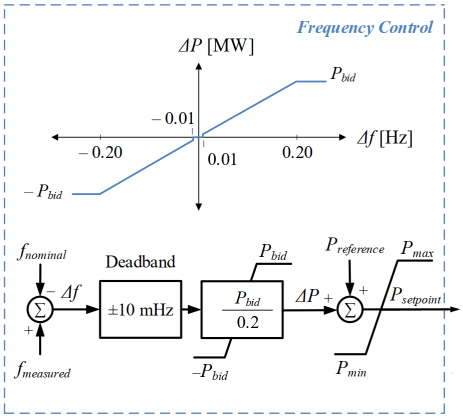

Figure 4.4: Droop controller for electrolyzer (retrieved from [66])

4.2.5. Electric Boilers

Electric boilers are used for steam production electrification to feed several high-temperature industrial processes within refineries, as discussed in detail in [15]. While different approaches can be used to model the thermal behavior inside the water tank of the boiler, the electrical power required from the grid to supply the necessary heat can be summarized as indicated in Equation 4.3.

$$\dot{Q}_{\text{heat}} = \frac{\eta}{100} \cdot P_{\text{elec}} \quad [\text{W}] \tag{4.3}$$

Where:

- $\dot{Q}_{\text{heat}}$ is the heat flow rate delivered by the heating element of the boiler in W
- η represents the efficiency of the electric boiler in %
- P_{elec} is the electrical power input in W

Furthermore, the heater can be regarded as a constant impedance load [38] [25]. Consequently, the rated power (P_{b} in W) of the boiler can be expressed as a function of its rated voltage (V_{b} in V) and the impedance of the heating element (R_{textb} in Ω) using the following relation:

$$P_{\text{b}} = \frac{V_{\text{b}}^2}{R_{\text{b}}} \quad [\text{W}] \tag{4.4}$$

Then, the actual electrical power input can P_{elec} can be rewritten as a function of the terminal voltage $V_{\text{t}})$ at which the boiler is connected to:

$$P_{\text{elec}} = \frac{V_{\text{t}}^2}{R_{\text{b}}} \quad [\text{W}] \tag{4.5}$$

Combining Equation 4.3, Equation 4.4, and Equation 4.5, the heat flow rate can be expressed in terms of the voltage terminal in the electrical network:

$$\dot{Q}_{\text{heat}} = \frac{\eta}{100} \cdot \left(\frac{V_{\text{t}}}{V_{\text{b}}}\right)^2 \cdot P_{\text{b}} \quad [\text{W}] \tag{4.6}$$

Two sizes of electrical boilers (i.e., 5 and 15 MW) are considered depending on their nominal power and voltage. In addition, PowerFactory's ZIP load model [67] [29] described by Equation 4.7 is implemented. It should be noted that the modeling is the same as in the case of the static loads mentioned in subsection 4.2.2. However, in some instances, it represented the aggregation of static loads within the low-voltage busbar of the installation, while in this case, each heater was independently

represented. The nominal ratings and parametrization of the electrical boilers implemented in the model are summarized in Table 4.5.

$$P = P_0 \left(aP \cdot \left(\frac{v}{v_0} \right)^{e_a} + bP \cdot \left(\frac{v}{v_0} \right)^{e_b} + (1 - aP - bP) \cdot \left(\frac{v}{v_0} \right)^{e_c} \right) \tag{4.7}$$

Table 4.5: Electric boiler parametrization in PowerFactory

Nominal Power (MW)	Nominal Voltage (kV)	a	b	c	e_a	e_b	e_c
5	6.3	0	0	1	0	0	2
15	25	0	0	1	0	0	2

4.2.6. Large Variable Speed Drive Interfaced Motors

Variable Speed Drives (VSDs) are crucial in the industrial sector due to their effective speed and torque control and contribution to energy efficiency. Commonly used in motors driving pumps, fans, or compressors, a VSD is installed between the electrical supply and the electrical motor. Firstly, it transforms the AC power supply to a DC bus through a rectifier. Secondly, capacitors reduce fluctuations on the DC bus while providing a stable DC supply. Finally, the inverter modulates the DC into AC with variable frequency and voltage. Such control is achieved through modulation techniques like Pulse Width Modulation (PWM), which enables the control of the motor's speed and torque output.

The DIgSilent PowerFactory VSD template [37] was adapted to feed a 30 MVA induction machine, representing the electrical drive of a large gas compressor. The initial model was intended for a 0.2 MW pump load. The electrical model includes the stages mentioned within a VSD: a rectifier, the internal capacitors, and the output inverter with PWM. Additionally, the template includes an AC/AC transformer to adapt the bus voltage to the input voltage required by the VSD and circuit breakers to control the supply to the VSD or the AC motor. Figure 4.5 shows the implemented model. From the template, the AC motor was substituted with a 30 MVA AC machine, while all the component ratings (i.e., voltage, current, and power) were adjusted to fit the new load. As the bus voltage matches the rectifier voltage rating, the input transformer was modified to be ideal (no losses), and a unitary voltage ratio was introduced. The transformer was kept to maintain its generic and adaptableness to different network ratings.

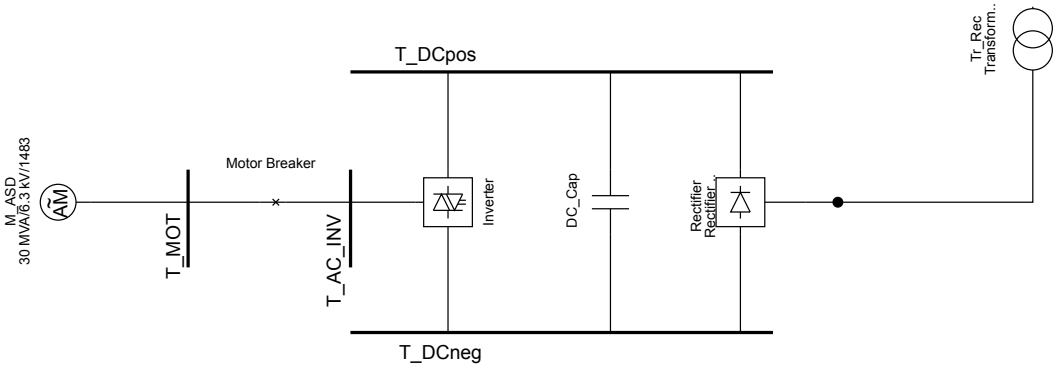

Figure 4.5: 30 MW Variable Speed Drive implementation in PowerFactory

Regarding the dynamic behavior of the load model, a PF composite model is considered within the template and was kept for the 30 MVA model. It includes a motor slot for sensing the speed and a mechanical machine slot where different load characteristics can be introduced. A compressor load characteristic substituted the original 0.2 MW pump load characteristic. Furthermore, a VSD main control slot measures the connection point variables (voltage supply, AC motor voltage, drive DC voltages, VSD, and motor breakers status) and the external speed setpoint. A V/f controller is set between the central VSD controller and the rectifier, providing a constant V/f ratio control. Finally, the PWM controller links the main VSD measurements with the output inverter. Overall, the control algorithm is implemented as an eight-state machine as depicted in Figure 4.6. A brief description of each state as defined in [37] is listed below:

- **S1 - Initialization:** While initializing the simulation, depending on the power flow results, the model will decide whether the results correspond to standstill or running conditions.
- **S2 - Standstill:** In this state, the drive is not energizing the motor (motor circuit breaker open). The motor is started when *start_command* variable is set to 1.
- **S3 - Network Monitoring:** When *start_command* variable is triggered, the VSD checks the AC power supply conditions. The motor will be energized if it is within the minimum and maximum set limits.
- **S4 - Motor Starting:** The motor starts ramping to reach its reference speed. Faults are triggered if the setpoint speed is not reached within a predefined time (*T_DETECT_STALLING*) or the motor or AC supply breakers are open.
- **S5 - Running:** Represents normal operation state. A fault state is triggered if the same events occur as in S4. In addition, if the network supply is out of the predefined limits during a certain time, the machine is transferred to a fault mode state.
- **S6 - Fault mode:** Reached when the motor is out of the boundary limits for normal operation.

Depending on the settings, this state exits by trying to reconnect to the network or reaccelerating the motor.

- **S7 - Shutdown:** After fault mode is reached a user-defined number of times, the VSD will be taken out of service by opening both circuit breakers.
- **S8 - Reacceleration:** It is used for automatic motor reacceleration after an AC side fault occurs.

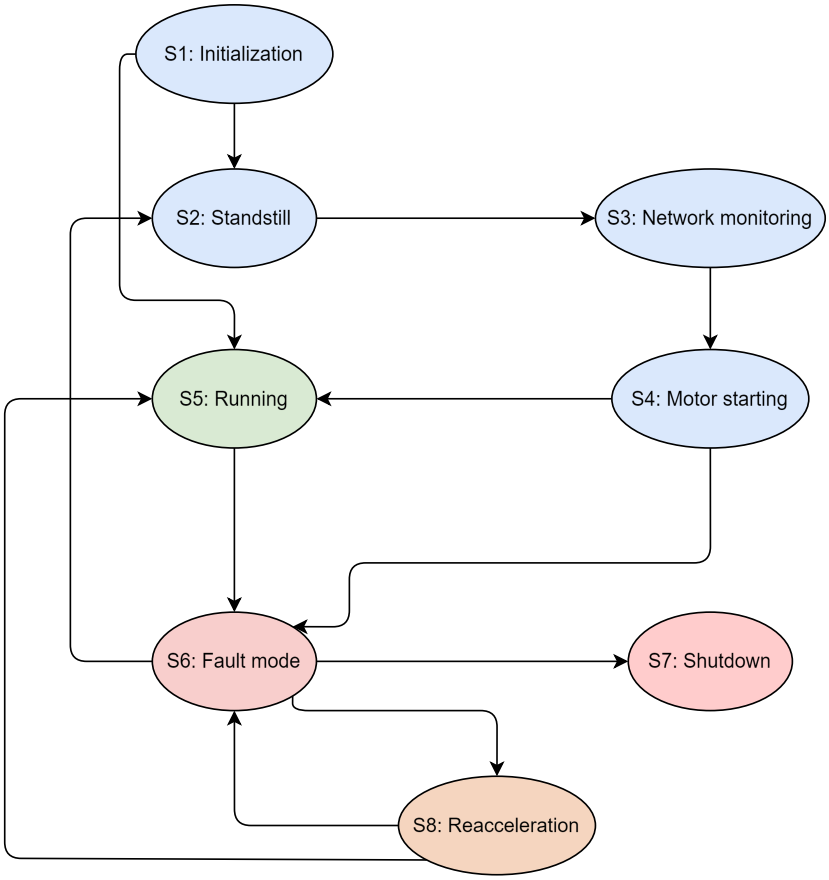

Figure 4.6: VSD implemented State Machine Flowchart

Table 4.6: VSD parametrization

Variable Name	Value	Unit	Description
SUPPORT_REACCELERATION	0	[0/1]	Support re-acceleration function
RECONNECT_COUNTER_MAX	5	-	Maximum number of motor starting re-trials before shutting down
U_MIN_CONNECT	0.95	p.u.	Minimum supply voltage at which motor may connect
U_MAX_CONNECT	1.05	p.u.	Maximum supply voltage at which motor may connect
U_MIN_SUPPLY	0.92	p.u.	Minimum allowed supply voltage during normal operation
U_MAX_SUPPLY	1.05	p.u.	Maximum allowed supply voltage during normal operation
W_STARTED_THRESHOLD	0.5	p.u.	Threshold for motor being considered as <started> at initialisation
W_BAND_STEADYSTATE	0.01	p.u.	Allowed band around speed reference
T_DETECT_STALLING	5	s	Stalling detection time
T_U_RECONNECT	5	s	Reconnect time after a fault (voltage monitoring)
T_W_RECONNECT	5	s	Reconnect time after a fault (speed monitoring)
T_MIN_W	1	s	Minimum time of steady state speed for entering normal operation
T_W_REACCELERATE	0.1	s	Minimum wait time before trying to re-accelerate
T_FAULT_U_SUPPLY	0.25	s	Maximum time at which supply voltage can exceed limits
T_FAULT_U_MOTOR	0.3	s	Maximum time at which motor voltage can exceed upper limit
T_FAULT_MAX_ALLOWED	10	s	Maximum fault period before shutting down
Fnom	50	Hz	Nominal grid frequency
WREF_MIN	0.01	p.u.	Minimum reference speed
GRD_WREF_DOWN	0.1	p.u./s	Speed reference gradient limiter (downwards)
WREF_MAX	2	p.u.	Maximum reference speed
GRD_WREF_UP	0.1	p.u./s	Speed reference gradient limiter (upwards)

4.3. Representation of Power Plant Dynamics

4.3.1. External Grid

The external grids linked to the 2A4G network utilize the PowerFactory *ElmXnet* component, designed to simulate external bulk systems. These components are fully parameterizable, facilitating adaptation to specific grid characteristics by representing various Thevenin equivalents observed from the grid connection point. Key parameters that will be modified to denote different grid strengths include the inertia constant (H), the short circuit current, and the secondary frequency bias.

The inertia constant was previously discussed in Chapter 3. The short-circuit current is directly configurable within the component settings. It is important to note that since the component modeling is based on aggregated synchronous generators, the nominal capacity of the grid is directly related to the short-circuit current. Therefore, this value can be as low as possible to ensure that the grid nominal capacity is sufficient for the power flow calculations to converge.

The SFB of the external grid is an auxiliary constant to compute the equivalent droop constant of the aggregated governors in the system. As the grid transitions from high SGs to RES, such value is expected to decrease. The mathematical representation is described as follows:

$$droop = SFB \cdot \frac{f_{\text{nom}}}{P_{\text{nom}}}[\%] \tag{4.8}$$

Where:

- SFB is an input parameter of the external grid, in MW/Hz
- f_{nom} is the nominal frequency of the grid in Hz
- P_{nom} is the nominal active power of the grid, at the nominal power factor, in MW

For further analysis, an equivalent droop characteristic of 12%, 2%, and 0% are considered. The first two are typical values for SGs [29], while the latter represents an extremely high penetration of power-interfaced energy sources. Consequently, the SFB will be set to 230, 40, and 0 MW/Hz, respectively.

4.3.2. Synchronous Generators (SGs)

In the modeled system, four identical SGs are integrated using PowerFactory's 46 MVA synchronous machine template. The dynamic behavior of these generators is enhanced by incorporating an exciter, a governor controller (GOV), and a power system stabilizer (PSS). The design of these controllers is in accordance with the guidelines found in [29], and their parameters are set based on the IEEE 421.5 standard [68].

Below is a concise description of each controller's function:

- **Exciter**: This controller's primary role is to adjust the generator's voltage output - the so-called Automatic Voltage Regulator (AVR). It achieves this by regulating the field voltage, thus controlling the terminal voltage and the machine's reactive power flow.
- **PSS**: The Power System Stabilizer assists the voltage regulator in mitigating oscillations within the power system. It modifies the generator field voltage using auxiliary signals such as shaft speed, frequency, or power. The current model employs rotor speed deviation as an input, aligning with

the practices described in [29].

- **GOV**: The governor, also known as the prime mover, regulates the conversion of thermal or hydro energy into mechanical energy, which drives the generator shaft to produce electrical energy. It facilitates the control of power and frequency via a power-frequency droop characteristic. Essentially, if the frequency declines, the governor increases mechanical power to the shaft, thereby boosting electrical output and vice versa.

Each controller plays a vital role in ensuring the stability and efficiency of the generator's operation within the power system. The interconnection between each controller is depicted in Figure 4.7, where:

- Vt is the generator terminal voltage
- w is the actual generator rotor speed
- w ref is the generator rotor speed reference
- Vpss is the stabilizing signal from the PSS controller
- P is the measured active power produced by the unit
- Ve is the field winding excitation voltage

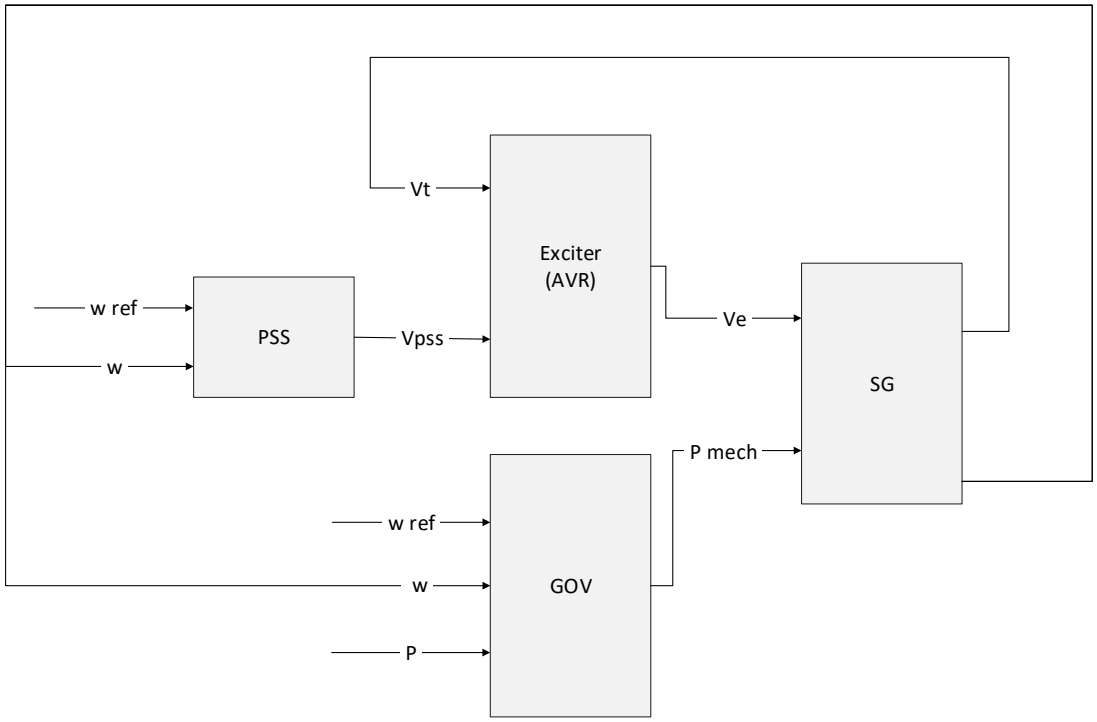

Figure 4.7: SG controllers schematic

4.3.3. Wind Power Plant (WPP)

In the case of the Wind Power Plant (WPP), the WECC 2 MW Full Converter Wind Turbine Type 4B is utilized. Detailed descriptions and specifications are in the documentation provided by WECC [69]. The model includes six parallel branches with controller parameters set to the typical values recommended by WECC [69]. Notably, frequency and voltage trips are disabled to focus on the load response characteristics.

Type 4 wind generators employ a back-to-back converter, isolating machine dynamics from the grid interactions. This configuration comprises AC/DC machine-side and DC/AC grid-side converters, ensuring all generated power passes through these power electronics, as illustrated in Figure 4.8. The operational setup is based on a grid-following approach, incorporating a phase-locked loop (PLL) that tracks the instantaneous angle of the busbar to which the WPP is connected. The real-time active and reactive power outputs are monitored against the reference values from a plant controller. The outputs from the power controller are then used to establish current setpoints in the *dq* frame, which aid the current controller in adjusting the output of the generator [70] [71].

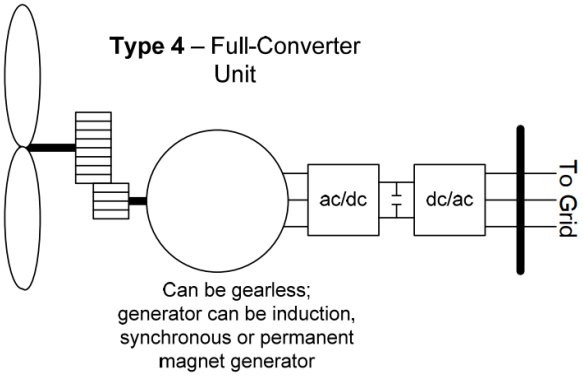

Figure 4.8: Full Converter Type 4 Wind Turbine schematic (retrieved from [69])

The control strategy within the WECC template model is implemented using three main controllers outlined below and schematically represented in Figure 4.9:

- **REGC_A**: This is the machine-side current controller, taking inputs of real and reactive current setpoints, with the output being the corresponding current injection into the grid.
- **REEC_A**: Acts as the power controller that handles active and reactive power setpoints received from the plant level control and determines the current references for the previous controller.
- **REPC_A**: This is the renewable energy plant controller, which processes measured grid voltage, power and reactive power references, and the network frequency. Its output, the power setpoints, are supplied to the power controller.

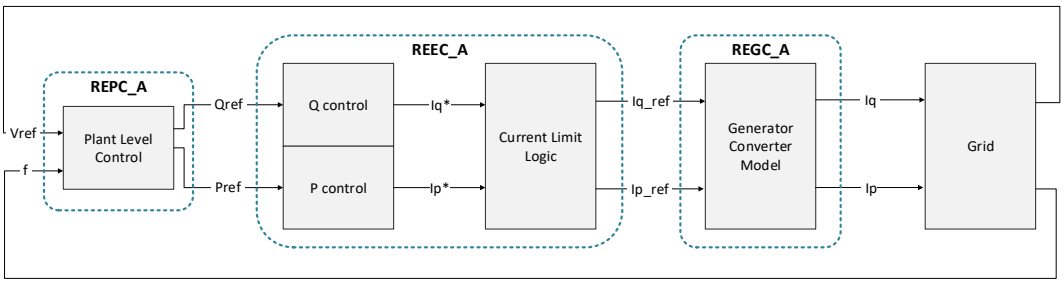

Figure 4.9: Block diagrams of WECC Type 4B Wind Power Plant controllers

4.4. Operational Scenarios and Analyzed Disturbances

4.4.1. Energy Supply Scenarios

Three scenarios have been created to explore how an industrial hub reacts to disturbances. Each scenario depicts a different setup of electricity supply for an industrial site, combining internal generation and power exchanges with the external grid. Scenario A reflects the current situation in the Pernis area,

where sites use their generators, such as Combined Heat and Power (CHP) units [15]. In addition, a marginal contribution of wind energy is considered, while the remaining power comes from the grid. Scenario B explores the effects of decommissioning SGs, focusing on how this impacts the system's short-term stability dynamics. Lastly, Scenario C examines a site that depends entirely on electricity supplied by the external grid. Table 4.7 depicts each energy supply scenario. The share is determined according to the demand that will be further explained in Table 4.9.

Table 4.7: Electricity source for Scenarios A, B, and C

Scenario	Electricity Source	Share (%)	Apparent Power (MVA)
A	SGs	35%	138
	Local WPP	15%	59.9
	External Grid	50%	196
B	SGs	0%	0
	Local WPP	50%	197
	External Grid	50%	196
C	SGs	0%	0
	Local WPP	0%	0
	External Grid	100%	393

4.4.2. External Grid Parametrization

The external grid is characterized according to three parameters: the total system inertia H (in seconds), the equivalent droop characteristic of the system named Secondary Frequency Bias (SFB in MW/s), and the short circuit current (in kA). The three parameters are highly affected by the introduction of inverter-based resources and the decommissioning of SGs. Consequently, it is expected that the three parameters will decrease over time [40] [41] [49], emphasizing the short-term frequency and voltage stability as the new technologies present a faster behavior.

The criteria described below are considered to characterize a strong, mid-strong, and weak grid representation. For the inertia constant, a high value of 7 seconds represents a grid with many thermal units (SGs) [29]. Then, 2 seconds to represent a limited inertia contribution, consistent with the inertia forecast in The Netherlands' National Trend 2040 scenario indicated in [40]. Finally, 0.5 seconds is considered for the weak grid as indicated in [43], corresponding to a high penetration of inverter-based technologies.

In the case of the SFB, it is parametrized according to the total load within the test network. Considering the 500 MVA generic industrial site and the auxiliary load of 1500 MVA previously discussed, the total load is around 2000 MVA. As the SFB refers to the aggregated frequency response of the system. When the energy is generated mainly by SGs, this value can be estimated as the aggre-

gated response of the governors within the system. Consequently, 12%/s and 2%/s with respect to the total load of the system are considered for the strong and mid-strong grid. This gives 240 MW/s and 40 MW/s, respectively. The aforementioned values for the droop constant are typically used as stated in [29]. A similar approach can be found in primary frequency response adequacy studies as in [48].

Finally, the short-circuit current of the equivalent external grid is determined. For the strong and mid-strong grid parametrization, the maximum and minimum short-circuit levels at 220 kV substations were considered. That is, 50 kA and 30 kA as indicated in [72]. Nevertheless, it should be pointed out that the model presents a limitation in setting the minimum value to represent the weak grid. On the one hand, as the external grid representation relies on an SG representation (as mentioned in subsection 4.3.1), the short-circuit current is related to the nominal capacity. Therefore, the short-circuit current can be set as low as the nominal capacity of the grid can supply the load. On the other hand, inverter-based generators provide an extremely low short-circuit current that depends on the controller's reactive current injection. Such current can be as low as 1.02 p.u. to the rated current of the converter, while usually in the range of 1.1 - 1.5 p.u. [73]. Despite this limitation, the study's objective is not to assess the exact dip present during a short-circuit event but to compare three cases to analyze the impact of decreasing fault levels. For such purposes, the model still allows assessing the results. The minimum fault level is set at 15 kA. A summary of each grid parametrization is indicated in Table 4.8.

Table 4.8: External Grid Characterization

Grid Classification	**H (s)**	**I_{cc}** (kA)	**SFB (MW/Hz)**
Strong	7	50	230
Mid-Strong	2	30	40
Weak	0.5	15	0

4.4.3. Load Demand

In addition to the supply mix and grid parametrization, the demand in the system will be the same for each scenario. In particular, every load in the system will be assumed to be operating at its nominal capacity, except for one electrolyzer. This asset will be set at its minimum technical operating point. By doing so, it is possible to simulate the contribution of ramping up hydrogen production while providing frequency containment reserves under different contingencies. In the same fashion, the electrolyzer operating at nominal capacity can ramp down in case of under-frequency conditions.

Table 4.9: Industrial load demand

Industrial load	Nominal Capacity (MVA)	Operating point (MVA)	Number of units	Initial demand (MVA)
Electrolyzer 1	155	31	1	31
Electrolyzer 2	155	155	1	155
Large electric boilers	15	15	3	45
Small electric boilers	5	5	6	30
VSD interfaced compressors	30	30	2	60
LV aggregated load	13	13	6	78

4.4.4. Considered Contingencies

Contingency analysis evaluates how the industrial site responds under various scenarios and with differing grid parameters. This analysis entails simulating an internal or external network disruption to assess the system's frequency and voltage responses. Each event is analyzed through multiple PowerFactory study cases, with the fault automatically activated at a preset time. A brief overview of the contingencies considered is provided below:

- **Grid Splitting**: In this scenario, Area 1, which contains the industrial hub, will be isolated from Area 2 by disconnecting two parallel transmission lines in the external grid. Before this event, Area 1 exported approximately 84 MW, which represented 4% of the total system load.
- **External Short-Circuit**: A three-phase short-circuit will occur on the 150 kV line entering the industrial site. A lengthy clearing time of 1 second is assumed, representing a scenario where the system fails to detect the fault promptly.
- **Industrial Site Internal Disturbances**: Two internal disturbances will be simulated, potentially leading to under-frequency issues due to power imbalance. For Scenario A, the outage of one SG is considered, while in Scenario B, it is the outage of one branch of the WPP. Each caused a loss of approximately 32 MW of power generation capacity. Additionally, an operation to ramp up an electrolyzer from 30 to 150 MW will be simulated. The analysis will largely focus on comparing the basic Scenario A against the most representative energy mix for large decarbonized industrial sites (i.e., Scenario B).

5

Analysis of Numerical Simulations

5.1. Methodological Approach

The impact of electrical network contingencies under various energy supply scenarios and external grid parameters is investigated using the following approach. Considering the technological shift in the electricity grid and the internal industrial assets, assessing the impact is paramount. Together with the increasing severe events due to climate change, it requires a thorough analysis to identify risks and mitigation measures.

Initially, the industrial hub is modeled in DiGSILENT PowerFactory, incorporating predefined network topologies, generation supply configurations, load component ratings and controllers, and a list of contingency events. Subsequently, a 20-second RMS simulation is conducted for each specified contingency, capturing data on electrical frequency, busbar voltages, active and reactive power, and load apparent power, which is exported to a CSV file. Performance metrics are then derived and analyzed using a Python script. An overview of the workflow is outlined in Figure 5.1.

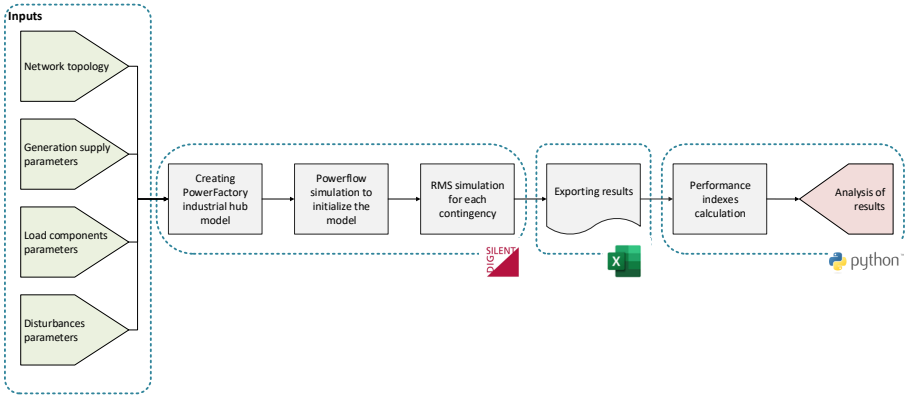

Figure 5.1: Methodological Approach

The initial assessment identifies the worst-case scenario, and mitigation strategies are proposed. Subsequently, new model parameters are established to incorporate these mitigation measures. The model is updated with the latest components or control strategies, followed by additional RMS simulations to evaluate performance metrics and the effectiveness of the proposed mitigations. This second assessment step is represented in Figure 5.2.

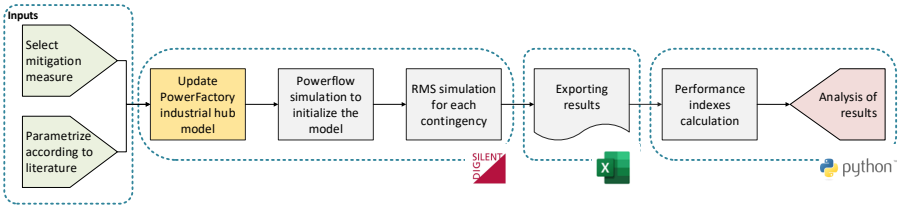

Figure 5.2: Methodological Approach for Mitigation Approaches

5.2. Performance Indexes

We have defined several indices to assess the system's short-term dynamic behavior, detailed in the following subsections. Each index is normalized against its maximum secure value. Consequently, 1 in any performance metric indicates the security threshold. Values below one are considered safe, whereas values exceeding 1 indicate a breach of technical requirements. For clarity in visualization, any index value exceeding 3.5 is capped at 3.5 on charts; however, this does not affect evaluating the results' severity.

5.2.1. Rate of Change of Frequency (ROCOF)

Mathematically, the ROCOF is the time derivative of the power system frequency [41]. It is measured immediately after a power imbalance and helps measure the system's inertia, as shown in Equation 3.5.

Therefore, it is a metric highly dependent on the SG units in the system, while wind or solar power plants cannot influence it [43]. In the context of the current research, the ROCOF will be calculated as the frequency difference over the first 500 ms after the disturbance, as shown in Equation 5.1, f_{d} corresponds to the frequency at the instant the disturbance was introduced, while $f_{\mathsf{d\,+\,500\,ms}}$ is the frequency 500ms after.

$$ROCOF = \frac{f_{\mathsf{d+500ms}} - f_{\mathsf{d}}}{500ms} \quad [\mathsf{Hz/s}] \tag{5.1}$$

Current operation limits are specified at 1 Hz/s, while new grid codes require new generation units to withstand up to 2.5 Hz/s [43]. The latter will be considered the boundary limit for a secure network operation. Consequently, the ROCOF metric will be normalized as follows:

$$Normalized\ ROCOF = \frac{ROCOF}{2.5Hz/s} \quad [-] \tag{5.2}$$

5.2.2. Maximum Frequency Deviation Index (MFDI) and Transient Frequency Deviation Index (TFDI)

The maximum frequency deviation (MFD) measures the maximum frequency excursion compared to the nominal frequency of the system (i.e., 50 Hz). It compares the minimum reached frequency -Nadir- or maximum frequency -Zenith- to the nominal frequency. Afterward, it is compared to the maximum tolerable transient excursion for each case, according to IEC 60034-1. In the case of the upward deviation, the limit is 1.03 p.u. (51.5 Hz), while downward is 0.95 p.u. (47.5 Hz).

$$MFDI = max\left[\frac{abs(Nadir - f_{\mathsf{N}})}{47.5Hz}, \frac{abs(Zenith - f_{\mathsf{N}})}{51.5Hz}\right] \quad [\text{-}] \tag{5.3}$$

Furthermore, the consecutive time the frequency is below the secure limits is measured. As no frequency-related relays are implemented in the model, this index will be used as an auxiliary metric to assess whether the deviation would cause an actual blackout. Under low-frequency events, part of the demand should be disconnected to restore the balance. Usually, measurement technology requires 5 to 8 cycles (100 to 160 ms) [74], while the load should be disconnected no more than 150ms after the command signal [47]. Consequently, 160 ms will be assumed as the maximum transient time the system can be below the acceptable limits without triggering a blackout. The normalized TFDI is shown in Equation 5.4. Note that for over-frequency events, the indicator is set to be one, assuming that the time the system can remain connected exceeds the analyzed time window. In case of over-frequency, disconnecting load can lead to further cascade events as the power imbalance increases, and so does the frequency deviation.

$$\text{Normalized TFDI} = \begin{cases} \frac{t_{\text{out of boundary limits}}}{160ms} & [\text{-}] \quad \text{for under-frequency} \\ 1, & \text{for over-frequency} \end{cases} \tag{5.4}$$

5.2.3. Post-fault Equilibrium Frequency

After the disturbance, if the system remains stable, the new frequency value at steady-state operation (f_∞) will be measured. For the continuous frequency operating point of the system, IEC 60034-1 establishes a range value of $\pm$ 1 Hz. Therefore, the post-fault frequency metric will be computed as follows:

$$\textit{Normalized Post-fault Frequency} = \frac{f_\infty - f_{\text{N}}}{1\,\text{Hz}} \quad [\text{-}] \tag{5.5}$$

5.2.4. Transient Voltage Deviation Index (TVDI)

The TVDI is a quantitative metric that helps to evaluate to what degree the voltage violates the secure limits and the corresponding time [75]. It is a helpful index as it considers the voltage deviation across the N busbars within the system for a given time window after the clearing time. Mathematically, it is represented as follows:

$$TVDI_{\text{i,t}} = \begin{cases} \frac{|V_{i,t} - V_{i,0}|}{V_{i,0}}, & \text{if } \left(\frac{|V_{i,t} - V_{i,0}|}{V_{i,0}} \geq \mu\right) \text{ for all } t \in [T_c, T] \\ 0, & \text{otherwise} \end{cases} \tag{5.6}$$

Where:

- i is the busbar number
- $V_{\text{i,0}}$ is the initial voltage at busbar i
- μ is the secure operating threshold (0.1 p.u. according to IEC 60034-1)

Then, the TVDI can be computed as described below:

$$TVDI = \frac{\sum_{i=1}^{N} \sum_{t=T_c}^{T} TVDI_{i,t}}{N(T - T_c)} \tag{5.7}$$

Where:

- N is the number of busbars in the system
- T_{c} is the time at which the fault was cleared

- T is the end time to assess the voltage deviation. Five seconds will be considered for this study.

To find an acceptable limit of the index, it is considered that the under- and over-voltage protections have a trigger time higher of 3.5 seconds, as indicated in the WECC load shedding guidelines [63] and implemented in the model. In addition, the simulation timestep is 0.01 seconds. Therefore, if the maximum voltage deviation allowed by IEC 60034-1 (i.e., 0.05 p.u.), and every bus deviates from its initial value for more than 3.5 seconds within the transient time frame ($T - T_c$), the maximum acceptable limit for TVDI results is 58.3. The normalized TVDI results will be as follows:

$$\textit{Normalized TVDI} = \frac{TVDI}{58.3} \quad [\text{-}] \tag{5.8}$$

5.2.5. Loss Load Index (LLI)

LLI is utilized to monitor the disconnection of loads in the industrial grid. Due to the close interrelation of each load with others in the production process, the disconnection of a single load can suddenly halt site operations. However, a cluster of loads that drive auxiliary processes may be considered non-critical. Taking such loads out of service does not impact the continuity of operation of the primary production process. The proportion of non-critical loads can vary, being lower in continuous processes and higher in batch processes within different industries. In this study, 10% (around 50 MVA) of the total demand load will be considered as non-critical. Thus, the index is calculated as:

$$\textit{Normalized LLI} = \frac{\text{Loss Load Power}}{\text{Non-critical Loads Nominal Power}} \quad [\text{-}] \tag{5.9}$$

5.3. Grid Splitting

5.3.1. Impact Across Scenarios

The first analyzed contingency is grid splitting. The initial power flow for such contingency is paramount, as it will determine the power imbalance of the system. As previously mentioned in subsection 4.4.4, Area 1 is exporting 84 MW to Area 2 to fulfill the power demand coming from the auxiliary Load B. The initial conditions are represented in Figure 5.3. After 2 seconds, both lines between the B3 and B2 external busbars are taken out of service. The over-frequency behavior of the site, consistent with the excess power in Area 1 after the splitting, is discussed below.

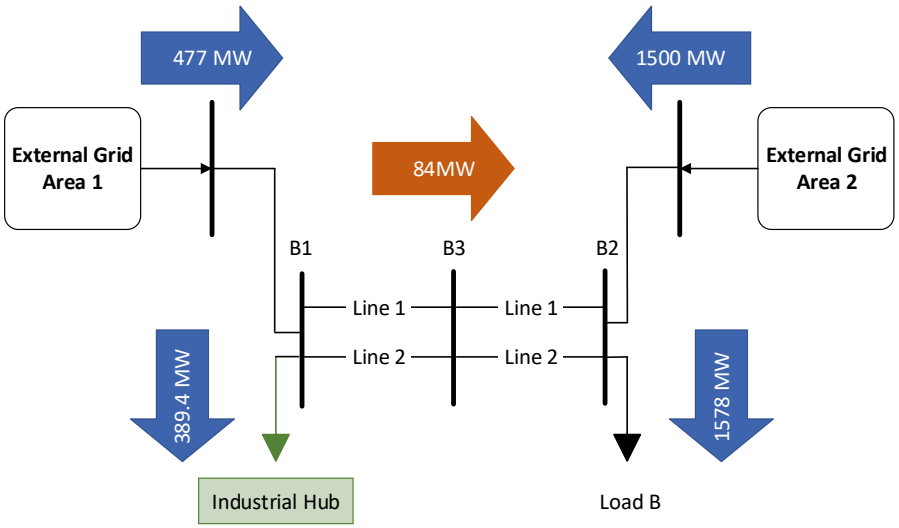

Figure 5.3: Grid splitting pre-fault power flow

The simulation results for each scenario are shown in Figure 5.4. The frequency is measured at the industrial hub incomer 150kV busbar (PCC with the external grid). The impact of different grid characteristics can be analyzed through the simulation. Firstly, the effect of a robust external network across the scenarios is remarkable. The high inertia in the system can be quantified by measuring the ROCOF. In every scenario, the ROCOF under a strong grid is below 0.2 Hz/s. However, when introducing a weak grid, such an index can be as high as 6.97 Hz/s. **This leads to an unstable condition in the case of Scenario C, meaning that the disturbance would lead to a sudden blackout of the industrial site when no local generators are present.** From the power system perspective, this cascade failure would exacerbate the power imbalance, requiring a trip of further generation facilities to regain the system's stability.

Secondly, for the secure operation of the industrial site, the post-fault frequency should be stable and within acceptable limits (i.e., 49 and 51 Hz). While the SGs are still in service (Scenario A), such objectives are quickly achieved. Nevertheless, **when substituting the SGs with a local wind power plant (Scenario B), the system is kept within acceptable limits. Still, it shows an oscillatory behavior and frequency deviation when connected to a weak grid. The risk of not stabilizing the frequency is that the system will be more susceptible to further disturbances.** This is due to the system's lack of frequency containment reserves and the WPP controller parameters. The first can be improved using an electrolyzer as a fast frequency response reserve. The latter is left out of the scope of the research.

Furthermore, in addition to the unstable condition when connected to a weak grid, the new equilibrium frequency for a mid-strong grid is out of the secure boundary limits. **If secondary frequency controllers, aiming to restore the variable to its nominal value, are not deployed on time, pro-**

tection relays will be tripped, leading again to a complete blackout of the industrial site. Again, introducing the electrolyzers as balancing reserves will be analyzed as a possible solution. In addition, power-to-heat equipment can also be used as a secondary frequency control depending on the severity of the deviation and the available time before tripping.

Finally, it should be emphasized that the most hazardous scenario arises when a site is entirely dependent on external grid electricity. Introducing local generators, such as thermal units or wind turbines, substantially enhances system stability. A thorough examination of the technical and economic aspects should be undertaken during the investment planning phases. Additionally, a probabilistic approach is necessary to evaluate the likelihood and frequency of the potential contingency. If grid splitting is likely to occur in the network, investing in local electricity generators becomes viable, considering the economic and technical risks involved. The radar chart in Figure 5.5 depicts the previous analysis. In the following subsection, a solution approach is introduced.

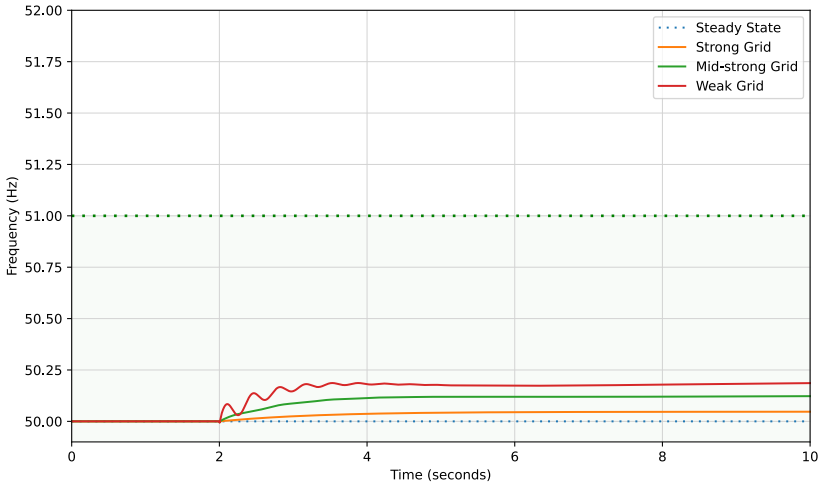

(a) Scenario A

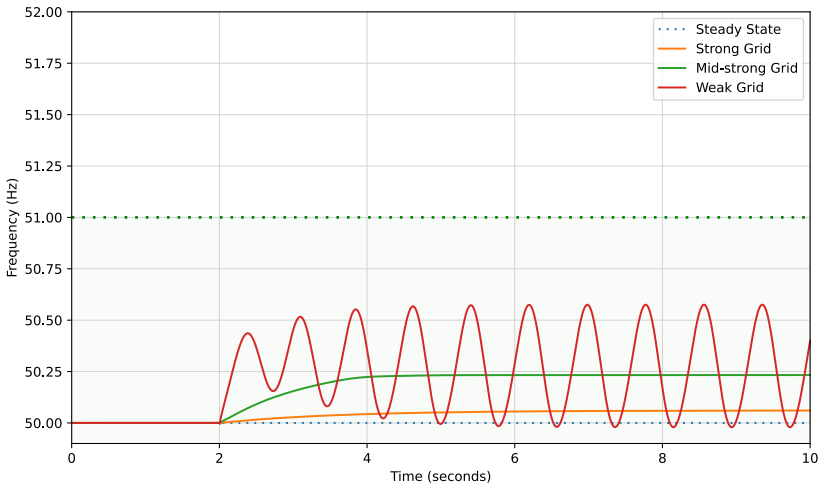

(b) Scenario B

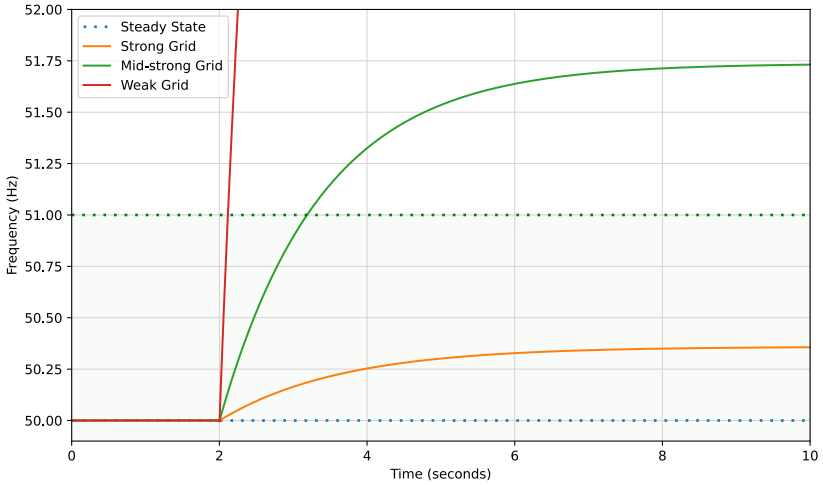

(c) Scenario C

Figure 5.4: Electrical frequency response to grid splitting (there is no derating on the industrial assets while operating in the green region)

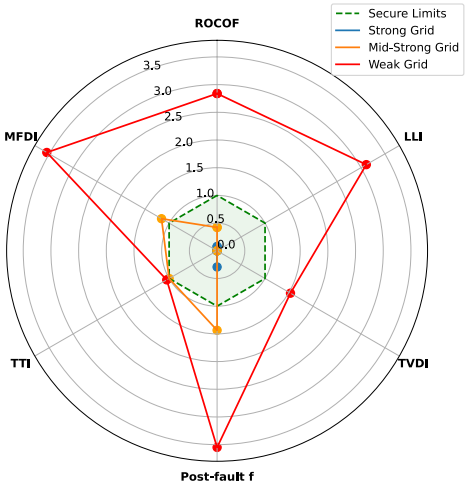

Figure 5.5: Performance index for grid splitting worst case (Scenario C)

5.3.2. Possible Mitigation Strategies and Solutions

To help withstand a splitting contingency, the electrolyzer is set to work as a frequency containment reserve. It is assumed that there is enough storage capacity to ramp up hydrogen production, so no limitations on the process side are present. The droop characteristic is enabled. The available parameters are shown in Table 5.1.

Table 5.1: Electrolyzer FCR control parametrization

Variable Name	Value	Unit	Description
FCR_db	0.2	Hz	FCR deadband
FCR_bid	120	MW	FCR bidsize
delta_f_max	1	Hz	Maximum FCR frequency deviation
P_ref	30	MW	Reference active power flow value
f_ref	50	Hz	Nominal frequency
grad	75	MW/s	Electrolyser ramp rate
Bid_min	-120	MW	Negative bid limit
P_min	30	MW	Electrolyser technical minimum active power
Bid_max	120	MW	Positive bid limit
P_max	150	MW	Electrolyser active power rating

Three different parametrizations are considered. As a starting point, a frequency deadband of 200 mHz is considered. This value is higher than typical governors' deadbands that can be around 100 mHz or even lower [48]. The higher this value is, the later the electrolyzer adjusts its power demand to control the system frequency. In addition, a ramping speed of 30% of the electrolyzer's nominal capacity per second is introduced. Then, the ramping rate is increased to the maximum rate available in the

PEM electrolyzer technology [27]. This rate is valid for an electrolyzer already in operation. Finally, the ramp rate is kept at the maximum feasible value, but the headband is reduced to 0.05 Hz. The three control strategies are summarized as follows:

Table 5.2: Electrolyzer FCR strategies for sensitivity analysis

Control Strategy ID	Description	FCR_{db}	Ramp rate (%/s)
LS-SR	Low Sensitivity - Slow Ramping	0.2	30
LS-FR	Low Sensitivity - Fast Ramping	0.2	50
HS-FR	High Sensitivity - Fast Ramping	0.05	50

The new curves are displayed in Figure 5.6, highlighting the significant impact of integrating one electrolyzer for FCR. This implementation allows the system to stabilize the frequency within secure limits. However, during conditions of slow ramping, the transient frequency excursions exceed acceptable thresholds for extended periods, potentially leading to a system blackout. Conversely, with faster ramping rates, the reduction in the headband correlates with lower frequency deviations. The revised indices for the three solutions are illustrated in Figure 5.7. Although the new approach enhances the post-fault frequency values, it marginally improves the ROCOF and the maximum frequency deviation after the fault. Nonetheless, it does not sufficiently shorten the transient times to bring them within acceptable limits.

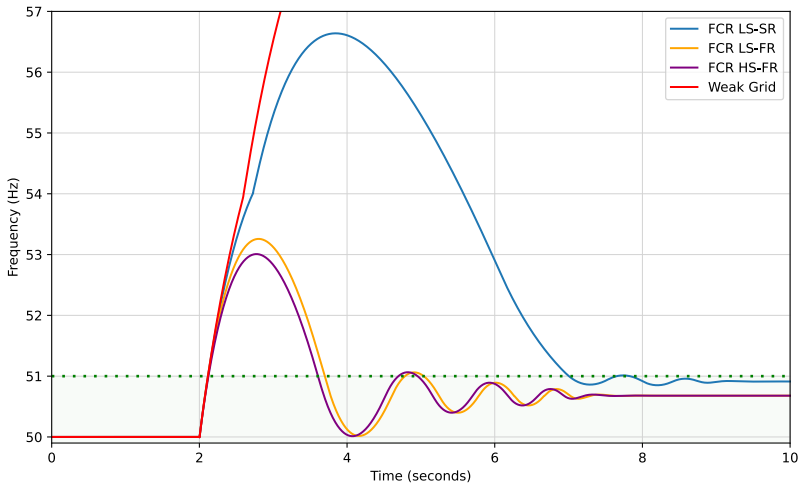

Figure 5.6: Frequency response under grid splitting with FCR

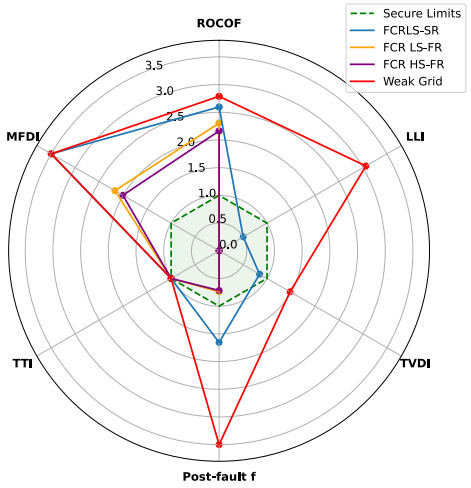

Figure 5.7: Performance index for grid splitting with FCR

To further improve the system's dynamic response, synchronous condensers are introduced into the model. The decommissioned SGs are turned into electric motors, while the inertia is modified to represent that it is not connected to the steam turbine. Two different inertia values are considered. First, one SC without any load is considered, with an inertia value of 2s. Then, a SC with a flywheel connected as a load is introduced. By doing so, the inertia of the machine is increased to 4 seconds. These are values consistent with available products as in [76]. The impact can be seen in

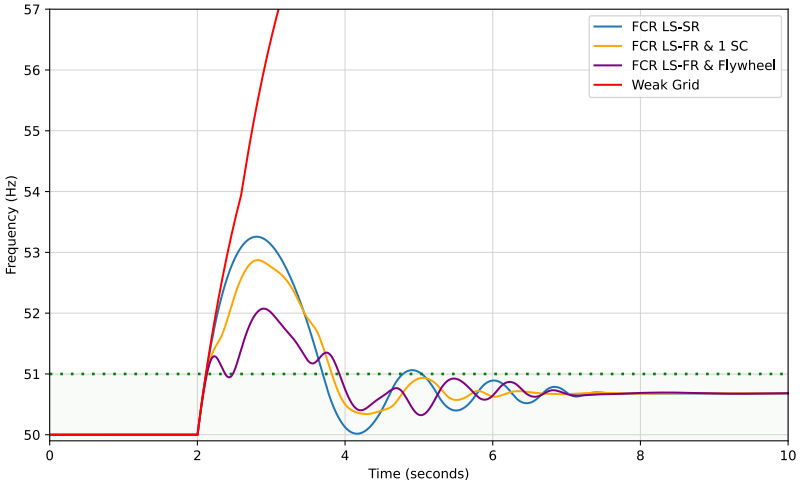

Figure 5.8: Frequency response under grid splitting with FCR

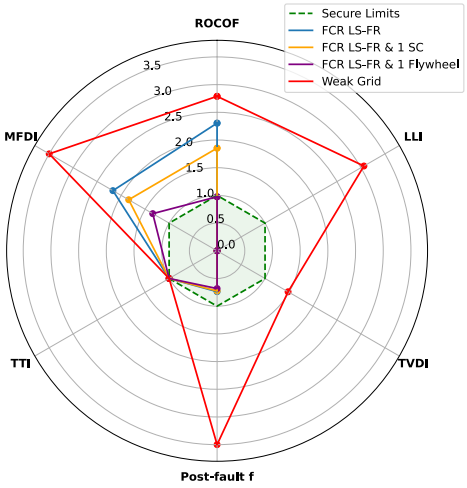

Figure 5.9: Performance index for grid splitting with FCR

To summarize, grid splitting represents a serious condition with potentially adverse effects on grid operators and connected loads. We have explored several solutions previously. Initially, we introduced a control strategy that utilizes an electrolyzer as a frequency containment reserve, equipped with droop-characteristic behavior. Additionally, a synchronous condenser and a flywheel were implemented to reduce the frequency excursion, thus further enhancing the security of the industrial electrical network. Combining these two approaches has proven an effective technical solution for severe frequency disturbances. It is important to note that implementing the control strategies will likely require less time and cost than introducing the hardware-based solution through a synchronous condenser or flywheel.

5.4. External Shortcircuit

5.4.1. Impact Across Scenarios

As mentioned, integrating inverter-based resources (IBRs) such as solar panels, wind turbines, and battery storage systems into power systems introduces new challenges. As traditional SGs are gradually replaced with these new technologies, there is a reduction in short-circuit levels in the external grid, drastically changing the dynamics and fault response of the grid. In addition, the short-circuit current (or power) is a metric closely related to the voltage stiffness of the grid [46]. Studying the impact of diminished short-circuit levels is crucial for ensuring the reliability, stability, and safety of power systems. An external short-circuit in the incoming 150 kV line is introduced after 5 seconds. The clearing time is set to be 1 second. The long clearing time simulates the impact of not detecting faults on time. As short-circuit levels are reduced, the protection relays detect the fault more slowly. The effect on the system stability is discussed as follows.

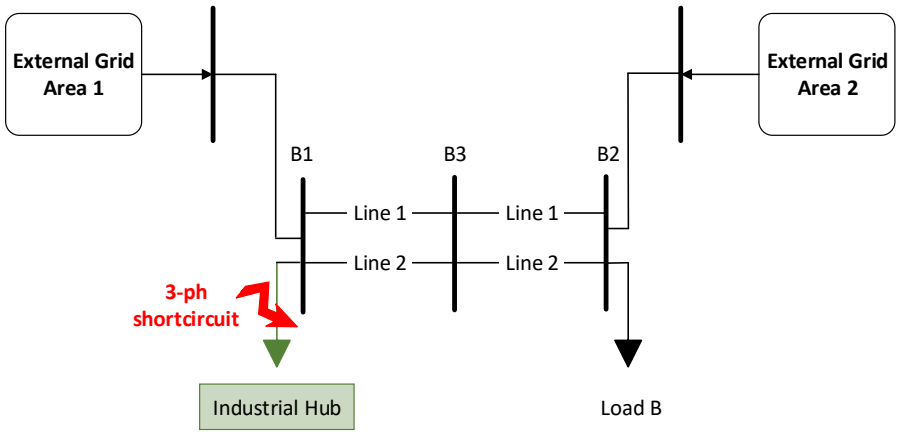

Figure 5.10: External shortcircuit location

To begin, the voltage will be monitored at one LV busbar. Given the meshed topology of the 25 kV internal distribution network, voltages are nearly the same at each busbar. However, due to the electrolyzer operating at peak capacity in Branch B, a slight reduction in voltage occurs, decreasing further at the radial 6.3 and 0.4 kV busbars. The impact of an external short circuit on voltage behavior is illustrated in Figure 5.11. Unlike grid splitting, Scenario B results in the most critical case. **Moreover, the local WPP fails to support system stability during the contingency**, resulting in a voltage dip to as low as 0.85 pu, below the LV loads' instantaneous overvoltage trip threshold. **This results in a loss load; that is, industrial assets are disconnected from the power supply.** Once the fault is cleared, the system's reduced power consumption causes a surge in voltage, almost reaching the upper continuous operation limit. This issue is exacerbated at the 6.3 and 25 kV busbars, where voltage levels exceed 1.05 pu.

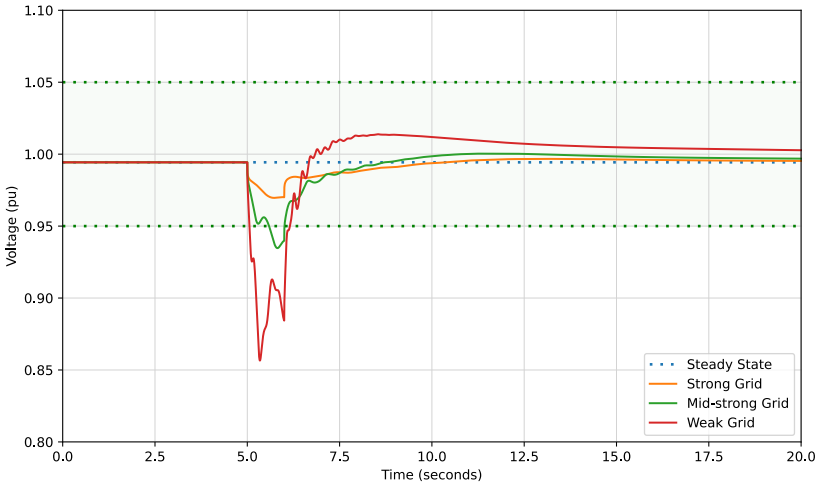

(a) Scenario A

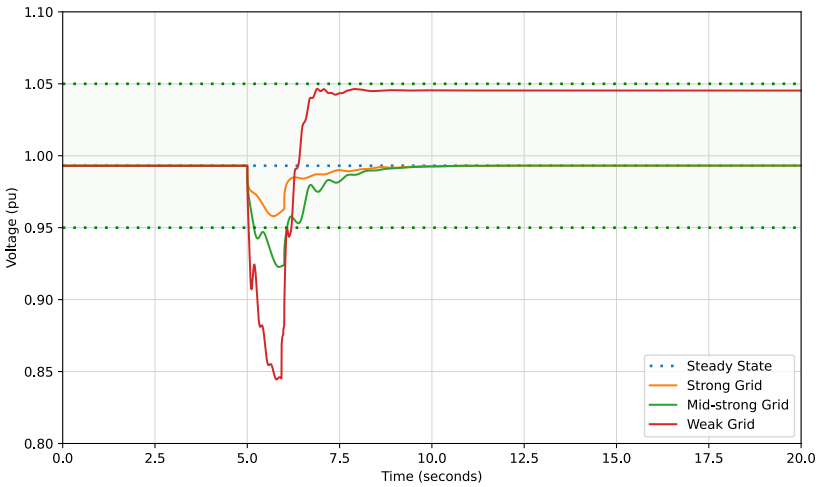

(b) Scenario B

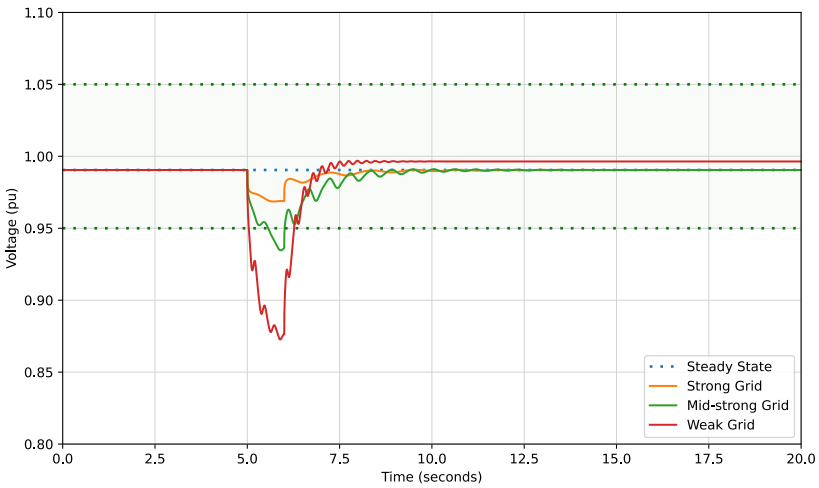

(c) Scenario C

Figure 5.11: 0.4kV Busbar B1 voltage during short-circuit contingency (there is no derating on the industrial assets while operating in the green region)

The radar charts in Figure 5.12 help further size each scenario's impact. With traditional SGs, although there is a slight overshoot beyond secure limits, voltage distortion quickly recovers with minimal frequency transients. In Scenario C, the weakness of the external grid is apparent, as it reaches insecure voltage and frequency levels. However, Scenario B presents the most severe issues, exacerbating voltage and frequency instability and leading to load losses accounting for around 15% of the total demand, nearly 1.5 times the maximum tolerable level, likely halting much of the production process. Considering that the load trips are due to undervoltage conditions, the following subsection will explore potential solutions to enhance resilience against short-circuit contingencies.

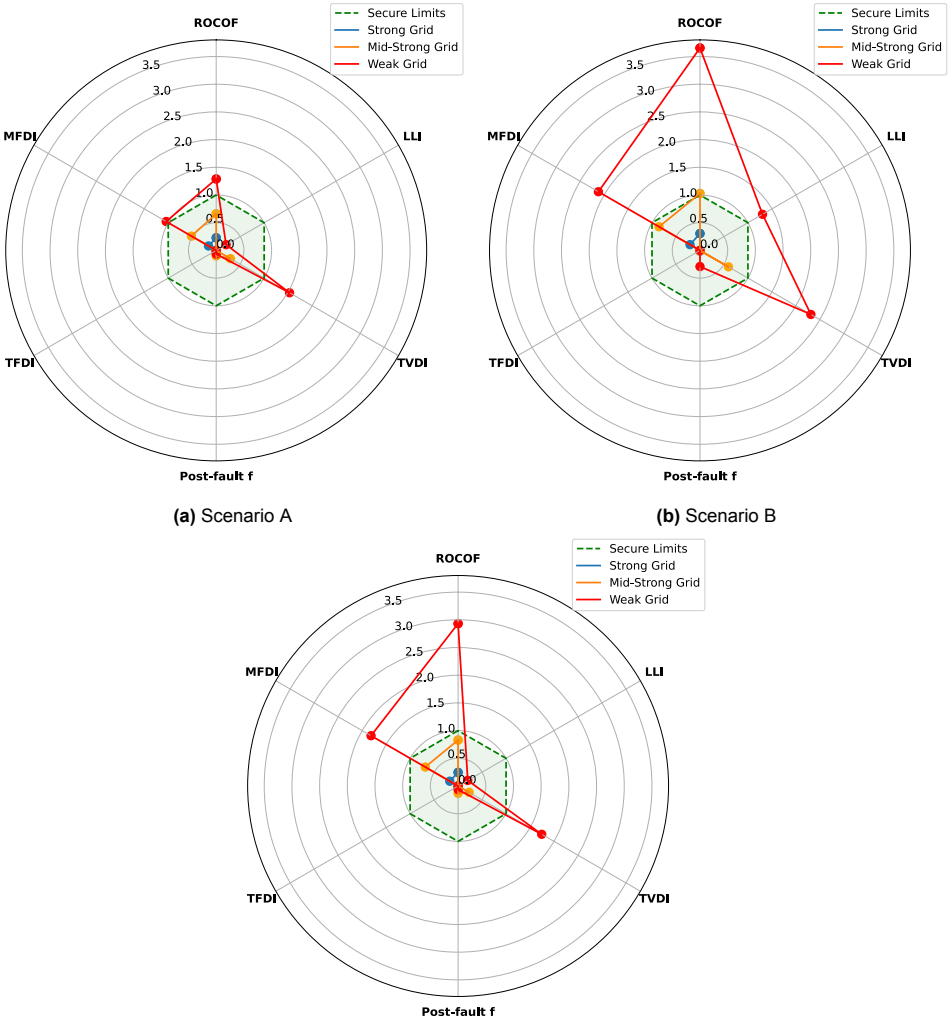

(a) Scenario A

(b) Scenario B

(c) Scenario C

Figure 5.12: Performance indexes under short-circuit contingency

5.4.2. Possible Mitigation Strategies and Solutions

This subsection discusses three different methods for addressing post-fault transients, each assuming that WPP control strategies remain unchanged, as optimizing the energy supply's control strategy is beyond the current research's focus. Instead, the emphasis is not on leveraging industrial assets to

enhance system stability.

The first approach involves converting a decommissioned SG into a Synchronous Condenser (SC). This conversion entails detaching the SG from its turbine, repurposing it as a synchronous motor, and updating its excitation system. Within the modeling tool, the transformation is achieved by reconfiguring the SC's designation from a generator to a motor, modifying the motor's inertia constant to 1.7 seconds to depict a machine operating without load [76], and adjusting the AVR tuning parameters. The latter is based on the parametrization implemented in [77]. These updated parameters are detailed in Table 5.3. Two SCs are retrofitted for the analysis.

Table 5.3: SC motor and controller parametrization

Variable Name	Value	Unit	Description
H	1.7	s	No-load inertia constant of the machine
K_a	150	pu	AVR exciter gain
T_a	0.3	s	AVR firing thyristor time constant
T_c	0	s	Lead time constant
T_b	0	s	Lag time constant

The second approach involves the integration of a flywheel with each SC. This method allows the exciter to continue managing the terminal voltage while the attached mechanical load stores kinetic energy, enhancing the overall system inertia. A flywheel installation results in an inertia constant of 16 seconds consistent with commercially available units [76]. The model is implemented by introducing the moment of inertia of the mechanical load to be 4500 $kg.m^2$. The updated parameters for the SC with flywheel are indicated in Table 5.4.

Table 5.4: SC with flywheel and controller parametrization

Variable Name	Value	Unit	Description
H	16	s	Inertia constant of the machine with flywheel
J	4500	$kg.m^2$	Flywheel (mechanical load) moment of inertia
K_a	150	pu	AVR exciter gain
T_a	0.3	s	AVR firing thyristor time constant
T_c	0	s	Lead time constant
T_b	0	s	Lag time constant

The third focuses on revising the trip settings for industrial loads to manage the sequence in which loads are disconnected during voltage drops while using only one SC. According to IEC 60034-1, induction machines can operate within a voltage range of 0.95 to 1.05 pu at rated values. Furthermore,

0.90 and 1.1 can be reached while derating the delivered torque. Therefore, the voltage trip thresholds were set at 0.92 and 1.08 pu, with a delay time of 3.5 seconds, with no distinction between critical and non-critical loads. The same parameters were used for the other components in the system.

The proposed load-shedding scheme updates these thresholds as outlined in Table 5.5. The primary goal of this strategy is to disconnect non-critical loads promptly once the secure operational limit is exceeded while allowing critical loads to continue operating even under lower voltage conditions. The feasibility of this approach depends significantly on the type of mechanical load driven by the electric motor. As voltage decreases, the motor's torque output lowers, as depicted in Figure 5.13, determining whether a new operating point is achievable based on the specific mechanical load characteristic.

Operating within an extended range is already feasible for loads interfaced with power electronics, as commercially available datasheets indicate. In the case of electric boilers, voltage fluctuations directly impact heat production. However, due to their thermal inertia, heating processes exhibit longer settling times, suggesting that short-term voltage instabilities are unlikely to disrupt their operation significantly.

Table 5.5: Load trip parameters for critical and non-critical loads

Trip Threshold (pu)	Delay (s)
Critical loads	
0.8	3.5
Non-critical loads	
0.95	0.5

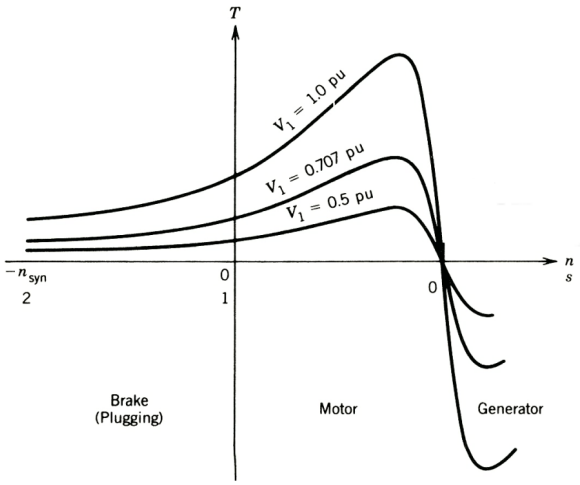

Figure 5.13: Induction machine torque derating depending on supply voltage (retrieved from [59])

Figure 5.14 shows the behavior under the newly implemented solutions. The reduction in

voltage dip is noticeable, bringing the lower value to around 0.92 pu. Implementing only SC or flywheels satisfactory brings the system to its nominal operating value after the disturbance, which means that no load was disconnected, and the power balance was restored after the fault was cleared. In the case of load shedding, it can be seen that the system starts to recover sooner than the other two solutions. This is due to the tripping delay time set to 0.5 seconds. The post-fault equilibrium is also improved, as it is further away from the upper secure limits, implying that less load was shed than in the base weak grid scenario.

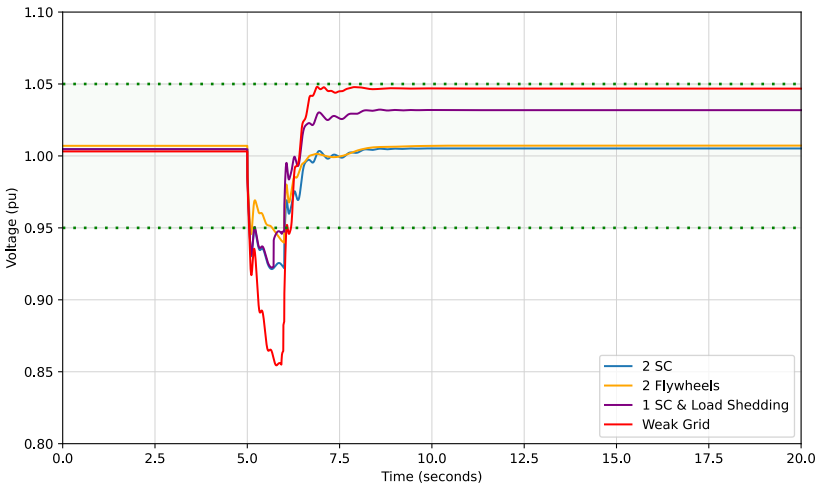

Figure 5.14: Voltage response to external shortcircuit

Nonetheless, comparing the transient behavior through the curve is challenging. To clarify, the radar charts illustrating the performance metrics of each solution are presented in Figure 5.15. The improvements are notably more apparent. Since each solution incorporates a synchronous machine, the system inertia is enhanced across all methods. However, their effects on voltage deviation transients vary. Both SC implementations with and without load shedding demonstrate similar outcomes, though the approach incorporating load prioritization slightly improves the TVDI and effectively eliminates frequency deviations. The LLI near 1 confirms that non-critical loads were disconnected. However, the optimal solution involves the addition of flywheels (refer to Figure 5.15b), which reduces every performance metric to the secure region, except for the ROCOF that remains marginally above 1.

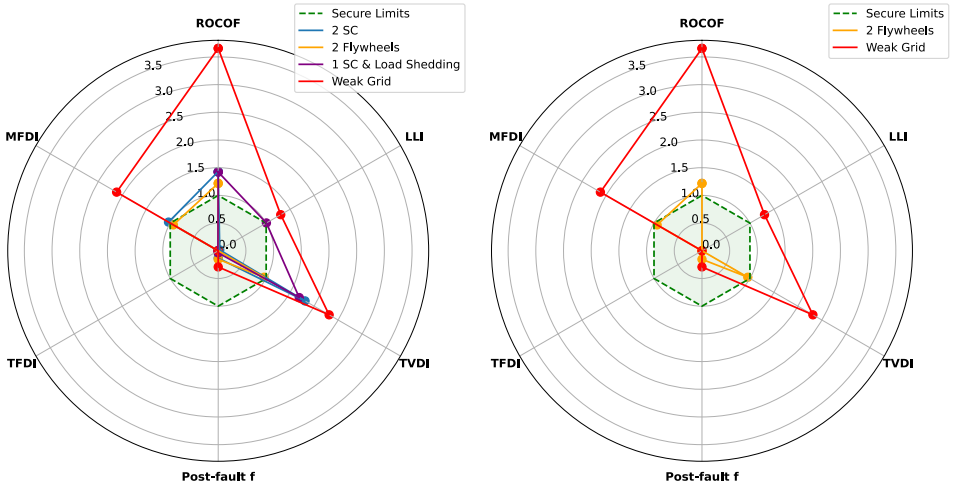

(a) Solution approaches comparison **(b)** Optimal solution compared to initial state

Figure 5.15: Performance indexes for possible solutions

Unlike grid splitting, where a controller-based approach already helps to improve the situation, the solution under a short-circuit scenario is not straightforward. The solution to withstand short-circuit conditions under a weak grid can include adding more equipment (synchronous condensers or flywheels), improving control (exciter of synchronous condenser to control reactive power), or reviewing the protection coordination of the loads. The most beneficial technology will depend on the process availability requirements, the probability of this type of failure in the specific power system, and the economics behind each solution. If the risk is high, investing in flywheels might be the best solution for more flexibility in the running hours, and the system's setup load shedding might be more cost-effective.

5.5. Internal Disturbances

5.5.1. Impact Across Scenarios

The discussion has focused on severe external disturbances and their effects on industrial sites. However, it is crucial to also analyze internal contingencies like power generation unit outages in light of new technologies. Moreover, the quick ramp rates of significant individual assets, though beneficial for balance support, may affect daily site operations. Therefore, this section and the next will examine and compare the dynamics of such internal disruptions. These contingencies will be introduced under two energy supply scenarios, comparing frequency and voltage responses. Subsequently, the worst-case scenario is examined, and solutions are discussed to mitigate disturbance effects.

For the upcoming analysis, we will consider Scenario A and Scenario B. Both scenarios allocate 50% of the energy supply from the external grid and 50% from internal generation units. In Scenario A, the 50% internal generation is divided between SGs (35%) and the WPP (15%). In Scenario B, the complementary energy supply comes entirely from the WPP. For the SGs, the N-1 operational

principle is represented. If one of the units goes out of service, the remaining operational assets compensate for one unit going offline. In the WPP, each branch runs at 80% of its capacity without the option of ramping up, simulating full wind energy utilization at the analyzed instant of time. Consequently, the external grid will provide the balance for the missing unit. Comparing the two scenarios, we will examine the outage of one SG in Scenario A and a branch outage of the WPP. Before setting the asset out of service, the faulty unit(s) deliver around 32 MW. Furthermore, we will simulate a daily operation where an electrolyzer ramps up from 30 MW to 150 MW, with a ramp rate of 50% of its total capacity per second (i.e., 75 MW/s). This implies an extra 120MW demand, with the site operating at peak capacity.

In Figure 5.16 and Figure 5.17, we compare each disturbance. The solid and dashed lines distinguish between Scenario A and Scenario B. Different colors on the curves help identify each contingency (generation outage in blue and electrolyzer ramp-up in orange). Observable differences exist in the power imbalances resulting from each disturbance. While the SG or WPP outage behaves similarly given that the power imbalance is almost the same (around 32 MW), **the sudden ramp-up of the electrolyzer in Scenario B significantly impacts frequency deviation. This shift places the new operating point beyond the secure limit. The faster dynamics of new industrial assets, such as the electrolyzer, require smooth and detailed operation planning to ensure secure limits are met.**

When analyzing voltage response, we observe that the faster WPP controller dynamics result in a slight voltage drop when a branch is set out of service. In contrast, an SG outage causes a more significant decrease. Nevertheless, the new operating conditions remain within safety parameters. As the electrolyzer load increases, the SG's PSS effectively limits voltage decay within operational limits and gradually improves system stability. Conversely, the voltage drop nears the lower limit for the WPP.

The active power control and voltage control controllers of the WPP must be tailored effectively when supplying power directly to an industrial site. This matter will be delved into further in the subsequent section.

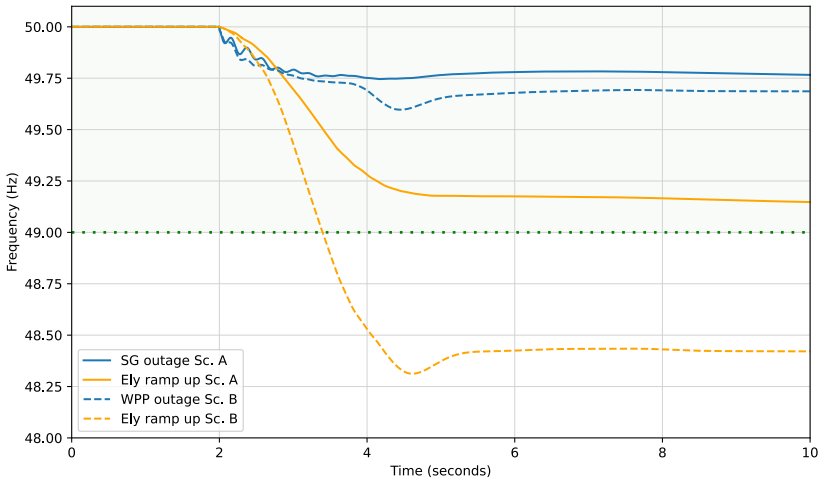

Figure 5.16: Frequency response comparison under different internal disturbances

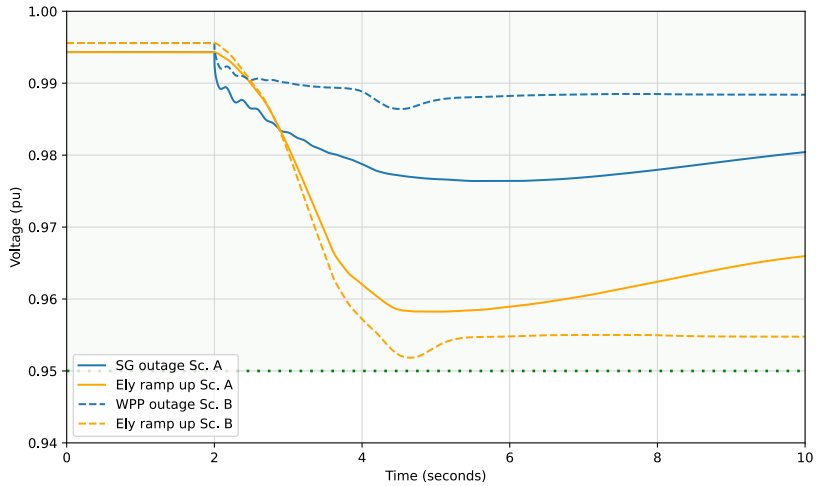

Figure 5.17: Voltage response comparison under different internal disturbances

5.5.2. Possible Mitigation Strategies and Solutions

In this case, only the ramping operation of the electrolyzer is discussed. As mentioned before, the operation of the industrial site should be carefully planned to keep the balance between generation and demand. Scenario B is a good approximation of future industrial sites: renewable energy resources will be near the industrial site to provide clean energy for decarbonized processes such as water electrolysis. Therefore, investigating the dynamics is of utmost importance.

In the initial conditions, each of the six branches of the WPP was operating at around 80% of its nominal capacity, with no ramping-up possibility. As a starting point, three different ramping rates are

depicted in Figure 5.18 and Figure 5.19 to help understand the impact. The new steady state frequency and voltage are the same in every case as the increase in the demand is fixed to an additional 120 MW. However, the faster the electrolyzer ramps up, the shorter the time window for balancing generation and demand is. **This implies a smooth and detailed coordination between the generation units and the industrial site operation.**

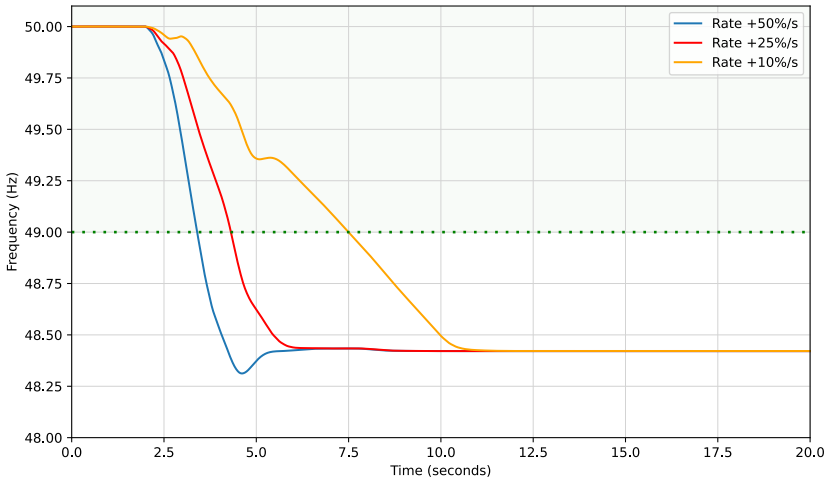

Figure 5.18: Frequency response for a coordinated operating between generation and load demand

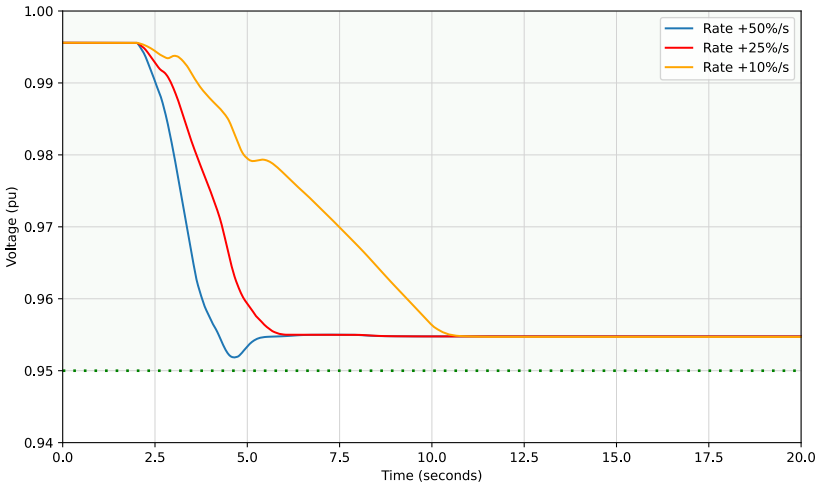

Figure 5.19: Voltage response for a coordinated operating between generation and load demand

The zero ramp-up assumption for the WPP is relaxed to delve further into the necessity of coordination. Starting from the same point at 80% of nominal capacity (192 MW for the WPP), we now assume the capability to ramp up WPP's active power to 100%. This adjustment allows for a ramp-up

rate of 1 pu/pu, meaning that for every additional 1 MW in demand, the WPP will supply an extra 1 MW, resulting in a 48 MW energy supply increase, reaching 240 MW supply.

Examining the impact of coordinating the electrolyzer ramp-up with available wind energy is demonstrated in Figure 5.20 and Figure 5.21. This coordination reduces energy imbalances, establishing a new secure operating point while limiting frequency and voltage deviations, even with the quicker electrolyzer ramp rate. Although this analysis is specific to a power imbalance scenario, the insights drawn are broadly applicable. **Smooth coordination of asset ramping based on distributed energy resource capacity is vital. Such coordination achieves two key objectives: ensuring clean energy-based production and enhancing operational site security.**

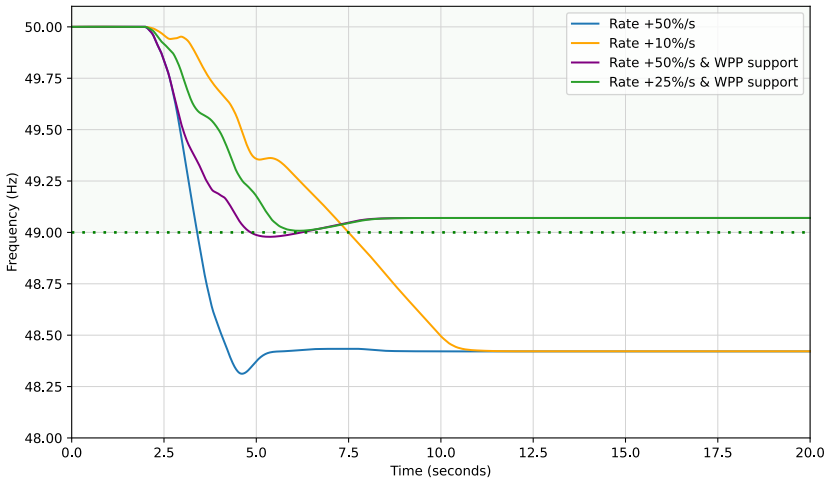

Figure 5.20: Frequency response for a coordinated operating between generation and load demand

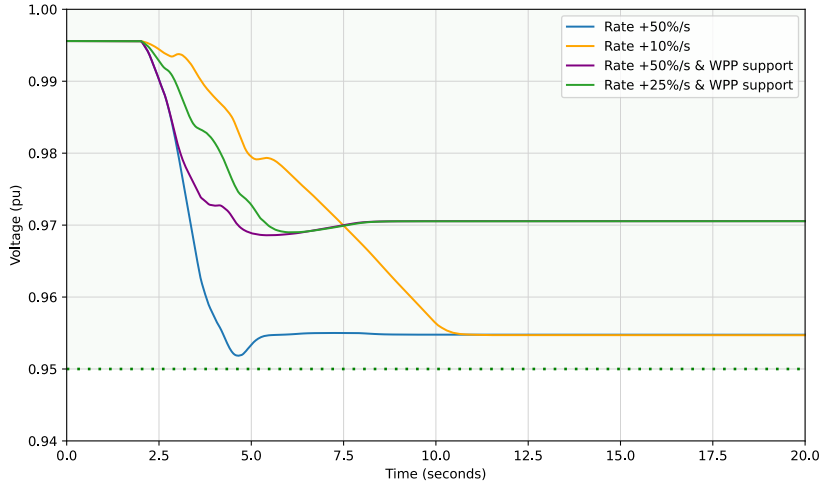

Figure 5.21: Voltage response for a coordinated operating between generation and load demand

5.5.3. Key Insights and Analysis Overview

This chapter delves into three disturbances: external grid splitting, three-phase short-circuit events, and internal operational disruptions. Each simulation's dynamic response was detailed, and potential mitigation strategies were discussed. The primary conclusions drawn from the results can be summarized as follows:

- External grid assessment should encompass more than just short-circuit power capacity. Collaboration between TSOs and industrial sites is crucial to exchanging information on bulk system inertia and available short-term balancing reserves.
- Severe frequency deviations like grid splitting can result in complete energy blackout for industrial sites. However, electrified sites with fast response equipment like electrolyzers or electric boilers can offer valuable balancing reserves, ensuring operational continuity.
- Voltage issues, such as those stemming from short circuits, are exacerbated by the integration of IBRs. Enhancing voltage control with reactive power controllers and reassessing electric asset withstand capabilities are vital considerations in future plans for low-carbon industrial sites.
- The balancing approach does not always require introducing new hardware. Retrofitting existing SGs as SC and fine-tuning asset controllers can be highly effective, even in critical conditions.
- Enhanced coordination between generation and demand entities - including TSOs and energy-intensive sites - is imperative. This collaboration should span short-term balancing reserves and incorporate day-ahead generation and demand forecasts based on wind and solar energy availability.

6

Conclusion

The ongoing energy transition introduces profound changes in power generation and consumption patterns within power systems. This shift is marked by a significant change in the dynamic behavior of electrical systems, where the response to identical disturbances varies considerably between traditional and future inverter-based power scenarios.

Industrial sites are at the forefront of this transformation, undergoing extensive modifications as they transition towards electrification by utilizing Power-To-Heat or Power-To-Gas technologies. Additionally, they are substituting fossil fuels with alternative energy carriers derived from renewable sources. This transition substantially challenges maintaining voltage and frequency stability across power networks, increasing the electricity demand while introducing faster dynamics.

Successfully navigating these changes requires a profound understanding of grid transient behavior and the potential for effectively managing industrial assets to ensure network stability. Such knowledge is crucial in making the energy transition secure, reliable, and cost-effective while maintaining the operational availability of assets.

There will be no single, universal solution, and the success of this transition will largely depend on collaboration among stakeholders, including industrial site managers, transmission system operators, and equipment manufacturers. Strong bonds and information exchange are required to achieve a reliable and sustainable decarbonization of the industrial sector.

6.1. Recap of Project Scope and Methodological Approach

6.2. Answers to Research Questions

What is a suitable digital model of an industrial hub to investigate its performance and interaction with an HV network under critical disturbances?

A suitable industrial hub digital model should seamlessly integrate hardware elements and software controllers within a unified network framework. This integration necessitates the adoption of component-based modeling, where key network elements such as busbars, transformers, motor and static loads, and power converter-interfaced loads are incorporated. Each component must allow for the easy modification of critical electrical parameters so that the model can quickly adapt to different scenarios and meet specific research goals with minimal effort.

Moreover, this model must include dynamic controllers tailored for time-domain simulations, enabling a comprehensive analysis of the industrial hub's interaction with the external high voltage (HV) network under various circumstances. It should come equipped with standard controller transfer function blocks, simplifying the creation of new control strategies. The model must also be capable of processing electrical signals like network frequencies or terminal voltages from different network components, adjusting responsively to operational setpoints — whether manually input by the user or automatically generated by the system. Critical actions that the model should perform include adjusting the active power output of generators or loads or altering the reactive current injection or generator consumption. This capability ensures a thorough examination of the hub's performance and its interactions during critical disturbances.

What is a proper modeling depth to simulate steady-state and dynamic responses of an industrial hub?

The appropriate modeling depth for simulating an industrial hub is affected mainly by the specific objectives of the research. The RMS simulation method was selected for this thesis to observe the system's transient dynamic response. This method demands a detailed representation of the electromechanical behavior of each component, focusing on their individual and aggregated responses during transient events.

A more profound exploration into power electronic modeling is essential for studies involving Electromagnetic Transients (EMT), where incidents such as lightning strikes or harmonic disturbances are a significant concern. This depth is crucial for accurately capturing the fast-paced dynamics of such transients, which is critical to effective analysis and the development of mitigation strategies. Precisely modeling protective devices' measurement capabilities and tripping settings is vital in protection coordination scenarios. Such detailed modeling is necessary to assess the reliability and safety of the

network during fault conditions.

While highly detailed models are valuable for studying systems under critical conditions, they require substantial computational resources. This level of detail might not always be necessary, particularly in studies like the one indicated in this report, where an RMS simulation is sufficient to assess the impact of network disturbances. In conclusion, a comprehensive yet adaptable modeling approach is vital. It should maintain an appropriate balance in modeling depth to successfully simulate an industrial hub's steady-state and dynamic behaviors when interacting with a high-voltage network under critical disturbances. Achieving this balance ensures that the model sufficiently represents reality to derive meaningful, qualitative conclusions from the study.

How to optimally manage the controllable assets of the industrial hub to ensure resiliency to both local and external disturbances?

The electrification and integration of power converter-based components introduce a new landscape of controllability within the industrial hub context. Droop characteristics, mimicking traditional governors, emerge as a promising control technique for Power-To-Gas equipment. The fast response of power electronics, coupled with the process flexibility to ramp up or down with minimal constraints, makes Power-To-Gas equipment well-suited to provide fast primary frequency response.

In larger time frames, Power-To-Heat technology can also play a key role in rapidly aiding the bulk system in restoring to nominal operating conditions. Moreover, technologies exhibiting inherent inertia, such as synchronous condensers and flywheels, might be a cost-effective solution to provide inertial response, regulate reactive power, and influence voltage levels through established controller mechanisms.

The optimal management and effectiveness of the industrial hub's assets will rely on several factors, including the power system's requirements, the economics behind each solution, and the smooth tuning of the controllers. Striking the right balance between these factors is crucial for maximizing the hub's resiliency to local and external disturbances.

Additionally, a comprehensive review of the secure operational limits of electrical assets is imperative. Given the evolving dynamics within the energy landscape and the unique challenges posed by the energy transition, a reassessment of asset protection strategies is essential. This reassessment aims to enhance operational continuity, extend the component lifespan, and safeguard the industrial hub's overall resilience.

6.3. Contributions

This thesis presents three distinct contributions. Firstly, a generic industrial electrical network topology has been developed to integrate the different electrified loads into one interrelated system. A representative industrial load mix has been implemented from a literature review of individual components. The model can be tailored for studies such as reliability assessments or cost optimization of industrial operations subjected to energy supply variability. This thesis demonstrates an application case related to contingency analysis based on RMS simulation. In addition, the network topology can be easily changed and adapted to represent different sites.

Secondly, a characterization of the external grid was proposed to represent the transformation due to the introduction of inverter-based technologies, such as wind and solar power plants. This characterization enables the simulation of the external grid over time, facilitating the analysis of the gradual integration of distributed renewable energy sources or the representation of different locations. A description of the impact of these technological changes is provided, including reduced inertia, low short-circuit levels, and a decrease in frequency reserves in the bulk system.

Severe contingencies were identified, and mitigation measures were proposed, implemented, and analyzed for effectiveness. These measures include operating the electrolyzer as a primary frequency reserve based on active power-frequency droop characteristics, implementing synchronous condensers and flywheels to improve reactive power injection for voltage control and enhance inertial response, and reviewing new protection configurations for industrial assets, prioritizing critical loads to ensure the continuity of operations.

6.4. Suggested Topics for Further Research

Future research on the following topics can follow the present thesis:

- **Grid operator and large industrial sites coordination to improve system reliability and balancing reserves**: electric network operators and industrial site managers should work closely to improve the information about system capabilities and potential collaboration for system stability. Electric planners from the industry will need more information than just the short-circuit power at the point of common coupling when planning the industrial site operation and protection schemes. On the grid side, new flexible and fast industrial assets can contribute to system balancing reserves, boosting the network's reliability.
- **Restoration control strategies based on Power-To-X technology**: Investigating control strategies to improve site availability under extreme conditions over long periods (days to weeks). This implies adding secondary frequency control strategies, mainly to Power-To-Heat assets.
- **Modeling of different load assets and electrical phenomena**: include other future electrified

loads such as data centers, electric vehicles, batteries, or fuel cells, and evaluate the dynamic behaviors and capabilities. In addition, the model can be tailored to analyze power converter phenomena such as harmonic distortion or unbalanced external faults.

References

[1] PBL Netherlands Environmental Assessment Agency. *Climate and Energy Outlook of the Netherlands 2022: English Summary of the Full Dutch Report 'Klimaat - En Energieverkenning 2022' (KEV)*. Tech. rep. PBL Netherlands Environmental Assessment Agency, 2022.

[2] Government of the Netherlands. *Climate Agreement [English Version]*. Tech. rep. Government of the Netherlands, 2019.

[3] European Comission. *Fit for 55: Delivering on the proposals*. URL: https://commission.europa.eu/strategy-and-policy/priorities-2019-2024/european-green-deal/delivering-european-green-deal/fit-55-delivering-proposals_en (visited on 03/08/2024).

[4] European Comission. *Energy Roadmap 2025: Impact assessment and scenario analysis*. Tech. rep. European Comission, 2011.

[5] International Energy Agency (IEA). *Tracking Industry*. URL: https://www.iea.org/energy-system/industry (visited on 03/08/2024).

[6] World Economic Forum. *The Future of Electricity: New Technologies Transforming the Grid Edge*. Tech. rep. World Economic Forum, 2017.

[7] B. De Metz-Noblat and G. Jeanjean. *Cahier technique nr. 185: Dynamic stability of industrial electrical networks*. Tech. rep. Groupe Schneider, 1997.

[8] C. Puret. *Cahier technique nr. 155: MV Public distribution networks throughout the world*. Tech. rep. Groupe Schneider, 1992.

[9] H. Devold. *Oil and Gas Production Handbook*. URL: https://new.abb.com/oil-and-gas/production-book/utility (visited on 03/18/2024).

[10] Kumar, Kumulainen, and Kauhaniemi. "Technical design aspects of harbour area grid for shore to ship power: State of the art and future solutions". In: *Electrical Power and Energy Systems* 104 (2019), pp. 840–852.

[11] *Networks*. URL: https://pandapower.readthedocs.io/en/v2.1.0/networks.html (visited on 10/18/2023).

[12] Ruiz Flores et al. *Assessment and planning of the electrical systems in Mexican refineries by 2014*. Tech. rep. Institute of International Education, 2011.

[13] R. Vafamehr. *Design of Electrical Power Supply System in an Oil and Gas refinery*. 2011.

[14] Omara and Nassar. *Voltage quality in delta Egypt network and its impact in oil industry*. Tech. rep. 2019, pp. 29–36.

[15] C. Oliveira and K. M. Shure. *Decarbonisation Options for the Dutch Refinery Sector*. Tech. rep. TNO and PBL Netherlands Environmental Assessment Agency, 2020.

[16] Valmet. *Valmet Recovery Boiler*. URL: https://www.valmet.com/pulp/chemical-recovery/recovery-boilers/ (visited on 10/20/2023).

[17] IEEE. *IEEE Std 141-1993: IEEE Recommended Practice for Electric Power Distribution for Industrial Plants*. Tech. rep. IEEE, 1993.

[18] Schneider Electric. *Electrical installation guide*. 2018.

[19] EATON. *Power Distribution Systems*. 2017.

[20] Parol et al. "Reliability Analysis of MV Electric Distribution Networks Including Distributed Generation and ICT Infrastructure". In: *Energies* 15 (2022), p. 5311. DOI: 10.3390/en15145311.

[21] Jordehi et al. "Industrial energy hubs with electric, thermal and hydrogen demands for resilience enhancement of mobile storage-integrated power systems". In: *International Journal of Hydrogen Energy* (2023). DOI: 10.1016/j.ijhydene.2023.07.205.

[22] AEMO. *PSSE models for load and distributed PV in the NEM*. Tech. rep. Australian Energy Market Operator, 2022.

[23] A. Boricic, J. L. Rueda Torres, and M. Popov. "Fundamental study on the influence of dynamic load and distributed energy resources on power system short-term voltage stability". In: *Electrical Power and Energy Systems* 131 (2021), p. 107141. DOI: 10.1109/ISGTAsia54193.2022.10003499.

[24] Z. Tang et al. "Dynamic Equivalent Model Considering Multiple Induction Motors for System Frequency Response". In: *Energies* 16 (2023), p. 2987.

[25] R. Sinha, B. Bak-Jensen, and J. R. Pillai. "Impact Assessment of Electric Boilers in Low Voltage Distribution Network". In: (2018).

[26] B. Tuinema et al. "Exploitation of Power-to-Gas for Ancillary Services Provision in the Netherlands". In: Cigré. 2019, pp. 1–17.

[27] José L. Rueda Torres et al. *Stability Analysis of an International Electricity System connected to Regional and Local Sustainable Gas Systems*. Tech. rep. Delft University of Technology, 2019.

[28] P. Mitra. *Improvements to load models and impact on system damping studies*. Tech. rep. Electric Power Research Institute, 2021.

[29] P. Kundur. *Power System Stability and Control*. 1st ed. Palo Alto, California: McGraw-Hill Inc., 1994.

[30] TenneT. *Netkaarten: Gird Map NL Onshore Corporate*. URL: https://www.tennet.eu/nl/ons-hoogspanningsnet/netkaarten (visited on 03/24/2024).

[31] ArcGIS. *TenneT Assets Hoogspanning*. URL: https://www.arcgis.com/home/item.html?id=02d4cfaf2a9241b68f9520748081d7e9 (visited on 10/11/2023).

[32] Port of Rotterdam. *Giant windmill on Maasvlakte 2*. URL: https://www.portofrotterdam.com/nl/nieuws-en-persberichten/reuzenmolen-op-maasvlakte-2 (visited on 03/24/2024).

[33] ib vogt. *Solarpark Scaldia*. URL: https://www.ibvogt.com/portfolio/solarpark-scaldia-2/ (visited on 03/26/2024).

[34] Hoogspanningsnet.com. *Regionale netschema's Nederland: 150 kV deelnet Botlek*. URL: https://www.hoogspanningsnet.com/netkaarten/regionaal/ (visited on 10/11/2023).

[35] P. Pillay, S. M. A. Sabur, and M. M. Haq. "A model for induction motor aggregation for power system studies". In: *Electric Power Systems Research* 42 (1997), pp. 225–228.

[36] WECC. *WECC Composite Load Model Specification*. Tech. rep. Western Electricity Coordinating Council, 2021.

[37] *Technical Reference: DIgSILENT Variable Speed Drive Template*. Tech. rep. DIgSILENT GmbH, 2023.

[38] R. Sinha et al. "Modelling of Hot Water Storage Tank for Electric Grid Integration and Demand Response Control". In: (2017). DOI: 10.1109/UPEC.2017.8231964.

[39] F. Oliveira. "AC Arc Furnaces Flicker Measurement without and with a SVC System Connected". In: *Renewable Energy and Power Quality Journal* 1 (2007), p. 05. DOI: 10.24084/repqj05.383.

[40] Christensen et al. *High Penetration of Power Electronic Interfaced Power Sources and the Potential Contribution of Grid Forming Converters*. Tech. rep. ENTSO-E, 2017.

[41] ENTSO-E. *Inertia and Rate of Change of Frequency (RoCoF)*. Tech. rep. Version 17. ENTSO-E, 2020.

[42] E. Orum et al. *Future system inertia*. Tech. rep. ENTSO-E, 2018.

[43] ENTSO-E. *System Needs Study: System dynamic and operational challenges*. Tech. rep. ENTSO-E, 1999.

[44] AEMO. *2024 General Power System Risk Review Approach Paper*. Tech. rep. Australian Energy Market Operator, 2023.

[45] L. Robinson D. Fracalossi. *Evaluating major contingencies and conditions with the potential to cause power system disruptions*. Tech. rep. Australian Energy Market Operator, 2024.

[46] M. Osman et al. *Short-Circuit Modeling and System Strength*. Tech. rep. North American Electric Reliability Corporation, 2018.

[47] EU-SysFlex. *State-of-the-Art Literature Review of System Scarcities at High Levels of Renewable Generation*. Tech. rep. European Comission, 2018.

[48] G. Kou et al. "Primary Frequency Response Adequacy Study on the U.S. Eastern Interconnection Under High-Wind Penetration Conditions". In: *IEEE Power and Energy Technology Systems* (2015).

[49] A. Boricic, J. L. Rueda Torres, and M. Popov. "System Strength: Classification, Evaluation Methods, and Emerging Challenges in IBR-dominated Grids". In: (2022).

[50] P. Makolo, R. Zamora, and T. Lie. "The role of inertia for grid flexibility under high penetration of variable renewables - A review of challenges and solutions". In: *Renewable and Sustainable Energy Reviews* 147 (2021), p. 111223. DOI: 10.1016/j.rser.2021.111223.

[51] I. Erlich, A. Korai, and F. Shewarega. “Study on the minimum share of conventional generation units required for stable operation of future converter-dominated grids”. In: *2018 IEEE Power Energy Society General Meeting (PESGM)* (2018). DOI: 10.1109/PESGM.2018.8585943.

[52] O. et al. *Plugging in: What electrification can do for industry*. Tech. rep. McKinsey Company, 2020.

[53] J. Oliveira and T. van Dril. *Decarbonisation options for the industry cluster Botlek/Pernis Rotterdam*. Tech. rep. TNO and PBL Netherlands Environmental Assessment Agency, 2022.

[54] T. Block, S. G. Palacios, and T. van Dril. *Decarbonisation options for large volume organic chemical production, Shell Pernis*. Tech. rep. TNO and PBL Netherlands Environmental Assessment Agency, 2020.

[55] M. A. Merkle and A. M. Miri. “Modelling of Industrial Loads for Voltage Stability Studies in Power Systems”. In: *Electrical and Computer Engineering Canadian Conference* 2 (2001), pp. 881–886.

[56] P. Bains et al. *Global Hydrogen Review 2023*. Tech. rep. International Energy Agency, 2023.

[57] ENTSO-E. *Scenarios descriptions and storylines*. URL: https://2022.entsos-tyndp-scenarios.eu/scenario-descriptions-and-storylines/ (visited on 04/25/2024).

[58] M. Couvreur et al. “The concept of short-circuit power and the assessment of the flicker emission level”. In: (2001).

[59] P. C. Sen. *Principles of electric machines and power electronics*. 2089.

[60] W. C. New and J. Berdy. *Load Shedding, Load Restoration and Generator Protection Using Solid-state and Electromechanical Underfrequency Relays*. Tech. rep. General Electric.

[61] IEA. *Emissions from Oil and Gas Operations in Net Zero Transitions*. URL: https://www.iea.org/reports/emissions-from-oil-and-gas-operations-in-net-zero-transitions (visited on 04/16/2024).

[62] Z. Ma et al. “Mathematical Representation of WECC Composite Load Model”. In: *Modern Power Systems and Clean Energy* 8 (5 2020).

[63] N. Shah et al. *Undervoltage Load Shedding Guidelines*. Tech. rep. Western Systems Coordinating Council, 2019.

[64] F. Alshehri et al. “Modelling and evaluation of PEM hydrogen technologies for frequency ancillary services in future multi-energy sustainable power system”. In: *Heliyon* 5 (2019). DOI: 10.1016/j.heliyon.2019.e01396.

[65] A. Buttler and H. Spliethoff. “Current status of water electrolysis for energy storage, grid balancing and sector coupling via power-to-gas and power-to-liquids: A review”. In: *Renewable and Sustainable Energy Reviews* 82 (1995), pp. 2440–2454.

[66] F. A. Alshehri. *Ancillary services from Hydrogen Based Technologies to Support Power System Frequency Stability*. 2018.

[67] DiGSILENT Power Factory. *Technical Reference Documentation: General Load*. Tech. rep. DIgSILENT GmbH, 2023.

[68] IEEE. *IEEE Recommended Practice for Excitation System Models for Power System Stability Studies*. Tech. rep. IEEE, 2005.

[69] WECC. *WECC Type 4 Wind Turbine Generator Model - Phase II*. Tech. rep. Western Electricity Coordination Council, 2013.

[70] T. Nguyen et al. “Grid-Forming Inverter-based Wind Turbine Generators: Comprehensive Review, Comparative Analysis, and Recommendations”. In: (2022).

[71] R. Wallace Kenyon et al. “Open-Source PSCAD Grid-Following and Grid-Forming Inverters and a Benchmark for Zero-Inertia Power System Simulations”. In: (2021).

[72] J. D. Glover, M. S. Sarma, and T. J. Overbye. *Power System Analysis and Design*. 4th ed. Thomson, 2008.

[73] R. Aljarrah, H. Marzooghi, and V. Terzija. “Mitigating the impact of fault level shortfall in future power systems with high penetration of converter-interfaced renewable energy sources”. In: *Electrical Power and Energy Systems* 149 (2023), p. 109058.

[74] AEMO. *Under Frequency Load Shedding: Exploring dynamic arming options for adapting to distributed PV: Victorian case studies*. Tech. rep. Australian Energy Market Operator, 2023.

[75] A. Boricic, J. L. Rueda Torres, and M. Popov. “Comprehensive Review of Short-Term Voltage Stability Evaluation Methods in Modern Power Systems”. In: *Energies* 14 (2021), p. 4076. DOI: 10.3390/en14144076.

[76] Andritz. *Boosting inertia of Synchronous condensers*. URL: https://www.andritz.com/hydro-en/hydronews/hn36/technology-flywheels (visited on 04/21/2024).

[77] S. Hadaviy et al. “A Robust Exciter Controller Design for Synchronous Condensers in Weak Grids”. In: (2021).

A

Source Code for Index Calculation

```python
import pandas as pd
import numpy as np

def calculate_rocof(filename, initial_time, final_time):
    # Load the dataset while skipping the first two rows (header rows)
    data = pd.read_csv(filename, skiprows=2)

    # Convert the 'Time' column to float, assuming the time values are numeric seconds
    data.iloc[:, 0] = pd.to_numeric(data.iloc[:, 0], errors='coerce')

    # Assuming the first column is 'Time' and the second is 'Frequency'
    times = data.iloc[:, 0]
    frequencies = data.iloc[:, 1]

    # Find indices for the specified time interval
    index1 = times.sub(initial_time).abs().idxmin()
    index2 = times.sub(final_time).abs().idxmin()

    # Get times and frequencies at these indices
    time1, freq1 = times[index1], frequencies[index1]
    time2, freq2 = times[index2], frequencies[index2]

    # Calculate delta time and delta frequency
    delta_time = time2 - time1
    delta_frequency = freq2 - freq1

```

```
    # Calculate ROCOF
    rocof = abs(delta_frequency / delta_time)
    Nrocof = rocof/2.5
    # print(f"ROCOF between {time1} and {time2} seconds: {rocof} Hz/s")
    print(f"Normalized ROCOF is: {Nrocof}")

    return rocof

def analyze_frequency_data(filename, nominal_frequency, tti_time):
    """
    Analyzes frequency data from a CSV file to determine various metrics.

    Parameters:
    - filename: str, the path to the CSV file containing Time and Frequency data.
    - nominal_frequency: float, the nominal frequency value for MFDI calculations.
    - tti_time: float, the time interval used for calculating TTI.

    Returns:
    - A dictionary with the calculated metrics: Nadir, Zenith, MFDI, TTI, f_inf.
    """

    # Read the CSV file
    data = pd.read_csv(filename, skiprows=2)

    # Convert Time and Frequency columns to appropriate data types
    data.iloc[:, 0] = pd.to_numeric(data.iloc[:, 0], errors='coerce')
    data.iloc[:, 1] = pd.to_numeric(data.iloc[:, 1], errors='coerce')

    # Extract time and frequency values
    time = data.iloc[:, 0].values*1000
    frequency = data.iloc[:, 1].values

    # Compute Nadir and Zenith
    nadir = np.min(frequency)
    zenith = np.max(frequency)

    # MFDI Calculation
    def calculate_mfdi(nadir, zenith, nominal):
        nadir_max = abs((nadir - nominal) / (nominal - 2.5))
        zenith_max = abs((zenith - nominal) / (nominal + 1.5))
        aux = max(nadir_max, zenith_max)
        if aux == nadir_max:
            N_mfdi = abs(nadir-nominal)/2.5
        else:
            N_mfdi = abs(zenith-nominal)/1.5
        return N_mfdi

```

```
    N_mfdi = abs(calculate_mfdi(nadir, zenith, nominal_frequency))

    # TTI Calculation
    def calculate_tti(frequencies, lower_bound, upper_bound, times, Td, T):
            # Check input parameters
        if Td >= T:
            raise ValueError("Td should be less than T")

        # Initialize variables
        count = 0
        time_above_threshold = []

        # Only consider times between Td and T
        valid_indices = [i for i, time in enumerate(times) if Td <= time <= T]

        # Calculate periods of time where frequency is outside the bounds
        for index in valid_indices:
            freq = frequencies[index]
            if freq > upper_bound or freq < lower_bound:
                if count == 0:
                    start_time = times[index]
                count += 1
            else:
                if count > 0:
                    end_time = times[index - 1]
                    time_above_threshold.append(end_time - start_time)
                    count = 0

        # Handle case where frequency stays out-of-bounds until time T
        if count > 0:
            end_time = times[valid_indices[-1]]
            time_above_threshold.append(end_time - start_time)

        # Calculate TTI if any times are recorded
        if time_above_threshold:
            tti_time = max(time_above_threshold)
            return tti_time
        else:
            return 0

    # f_inf Calculation
    def calculate_f_inf(data):
        steady_states = []
        for idx in range(2, len(data)):
            if abs(data[idx] - data[idx - 1]) < 0.0001 and abs(data[idx - 1] - data[idx - 2])
                 < 0.0001:
                steady_states.append(data[idx])
```

```
        if steady_states:
            return np.mean(steady_states)
        else:
            return None

    f_inf = calculate_f_inf(frequency)
    Nf_inf = abs(f_inf-nominal_frequency)
    tfdi = 1000*calculate_tti(frequency, 47.5, 51.5, time/1000, 2, 5)
    Ntfdi = 1000*calculate_tti(frequency, 47.5, 51.5, time/1000, 2, 5)/160

    # print(f"Nadir: {nadir} Hz")
    # print(f"Zenith: {zenith} Hz")
    # print(f"f_inf: {f_inf if f_inf is not None else 'No stable f_inf found'}")
    print(f"N_MFDI: {N_mfdi}")
    print(f"Normalized TFDI: {Ntfdi}")
    print(f"Nf_inf: {Nf_inf if f_inf is not None else 'No stable f_inf found'}")
    # print(f"MFDI: {mfdi}")

    # Package results into a dictionary and return
    return {
        "Nadir": nadir,
        "Zenith": zenith,
        "MFDI": N_mfdi,
        "TFDI": tfdi,
        "f_inf": f_inf
    }


def analyze_voltage_profiles(filename):
    # Read the dataset, assuming the first two rows are headers
    data = pd.read_csv(filename, skiprows=2)
    data.index = pd.to_datetime(data.index)

    # Dictionary to specify column ranges for each voltage level
    voltage_columns = {
        0.4: data.iloc[:, 1:7],
        6.3: data.iloc[:, 7:9],
        25: data.iloc[:, 9:12],
        150: data.iloc[:, 12:13]
    }

    # Prepare to collect results
    results = {}

    # Process each voltage level and its assigned columns
    for voltage_level, columns in voltage_columns.items():
        max_voltage = columns.max().max()
```

```
        min_voltage = columns.min().min()

        busbar_max = columns.max().idxmax().split()[0][:2]
        busbar_min = columns.min().idxmin().split()[0][:2]

        durations_above = {}
        durations_below = {}
        for column in columns.columns:
            busbar_code = column[0][:2]

            times_above = (columns[column] > 1.05 * voltage_level).astype('int')
            times_below = (columns[column] < 0.95 * voltage_level).astype('int')

            duration_above = (times_above * (times_above.groupby((times_above != times_above.
                shift()).cumsum()).cumcount() + 1)).max()
            duration_below = (times_below * (times_below.groupby((times_below != times_below.
                shift()).cumsum()).cumcount() + 1)).max()

            durations_above[busbar_code] = duration_above
            durations_below[busbar_code] = duration_below

        worst_above = max(durations_above, key=durations_above.get)
        worst_below = max(durations_below, key=durations_below.get)

        results[voltage_level] = {
            'Maximum Voltage': max_voltage,
            'Busbar for Max Voltage': busbar_max,
            'Minimum Voltage': min_voltage,
            'Busbar for Min Voltage': busbar_min,
            'Max Duration Above 1.05 times': (worst_above, durations_above[worst_above]),
            'Max Duration Below 0.95 times': (worst_below, durations_below[worst_below])
        }

    # Print results
    for level, res in results.items():
        print(f"Voltage Level: {level} kV")
        print(f"Maximum Voltage: {res['Maximum Voltage']} on Busbar: {res['Busbar for Max
            Voltage']}")
        print(f"Minimum Voltage: {res['Minimum Voltage']} on Busbar: {res['Busbar for Min
            Voltage']}")
        print(f"Maximum Time Above 1.05 times: {res['Max Duration Above 1.05 times'][1]} at
            Busbar: {res['Max Duration Above 1.05 times'][0]}")
        print(f"Maximum Time Below 0.95 times: {res['Max Duration Below 0.95 times'][1]} at
            Busbar: {res['Max Duration Below 0.95 times'][0]}\n")

    return results

```

```
208 def calculate_load_trip(filename, margin):
209     data = pd.read_csv(filename, skiprows=2)  # Considering headers are in both rows
210 
211     # Set the first row as the column names
212     data.columns = data.iloc[0]
213 
214     # Drop the first row (headers)
215     data = data[2:]
216 
217     # Convert apparent power columns to numeric values
218     data.iloc[:, 1:] = data.iloc[:, 1:].apply(pd.to_numeric, errors='coerce')
219 
220     # Get the number of loads
221     num_loads = len(data.columns) - 1  # Subtract 1 for the timestamp column
222 
223     # Initialize total tripped load difference
224     total_trip_difference = 0
225 
226     # Calculate the difference for each load
227     for load in range(3, num_loads + 1):  # Start from column 1 (load 1)
228         initial_power = data.iloc[0, load]
229         final_power = data.iloc[len(data) - 1, load]
230 
231         # Calculate the percentage difference
232         power_difference = abs(final_power - initial_power)
233         if power_difference > margin/100 * initial_power:  # Check if the difference is
                higher than the specified margin
234             total_trip_difference += power_difference
235 
236     LLI = total_trip_difference/50
237     # print(f"Total loss power: {total_trip_difference} MVA")
238     print(f"Loss␣Load␣Index:␣{LLI}")
239 
240     return total_trip_difference
241 
242 def calculate_tvdi(filename, Tc, T, mu):
243     # Read the CSV file into a DataFrame
244     data = pd.read_csv(filename, skiprows=2)  # Skip the first two header rows
245 
246 
247     # Get the number of buses (N)
248     N = data.shape[1] - 1  # Subtract 1 for the timestamp column
249 
250     # Get the time data from the first column
251     time_data = data.iloc[:, 0].values
252     # time_data =  data[:,0]
253 
```

```
    # Find the initial voltage (Vi,0) for each bus
    initial_voltages = data[time_data >= 0].iloc[0, 1:].values

    # Calculate TVDI_i,t for each bus
    tvdi_it = []
    for i in range(N):
        # bus_voltages = data.iloc[:, i+1].values
        bus_voltages = data.iloc[:, i+1]
        tvdi_it.append([])
        for t in range(len(bus_voltages)):
            if time_data[t] >= Tc and time_data[t] <= (Tc+T):
                if (abs(bus_voltages[t] - initial_voltages[i])/initial_voltages[i]) >= mu:
                    tvdi_it[i].append((abs(bus_voltages[t] - initial_voltages[i])/
                        initial_voltages[i]))
                else:
                    tvdi_it[i].append(0)

    # Calculate TVDI
    tvdi = sum([sum(tvdi_it[i]) for i in range(N)]) / (N * T)
    Ntvdi = tvdi/20

    # print(f"The Transient Voltage Deviation Index is: {tvdi} ")
    print(f"The Normalized Transient Voltage Deviation Index is: {Ntvdi} ")
    return tvdi
```

B

DIgSILENT PowerFactory Components

The implemented network topology is shown in Figure B.1. It can be modified by opening or closing the circuit breakers or setting the different components out of service.

Coupled with different transmission grid representations, the incoming transformers can be modified by adjusting the voltage and power ratings, as schematically pointed out in Figure B.2.

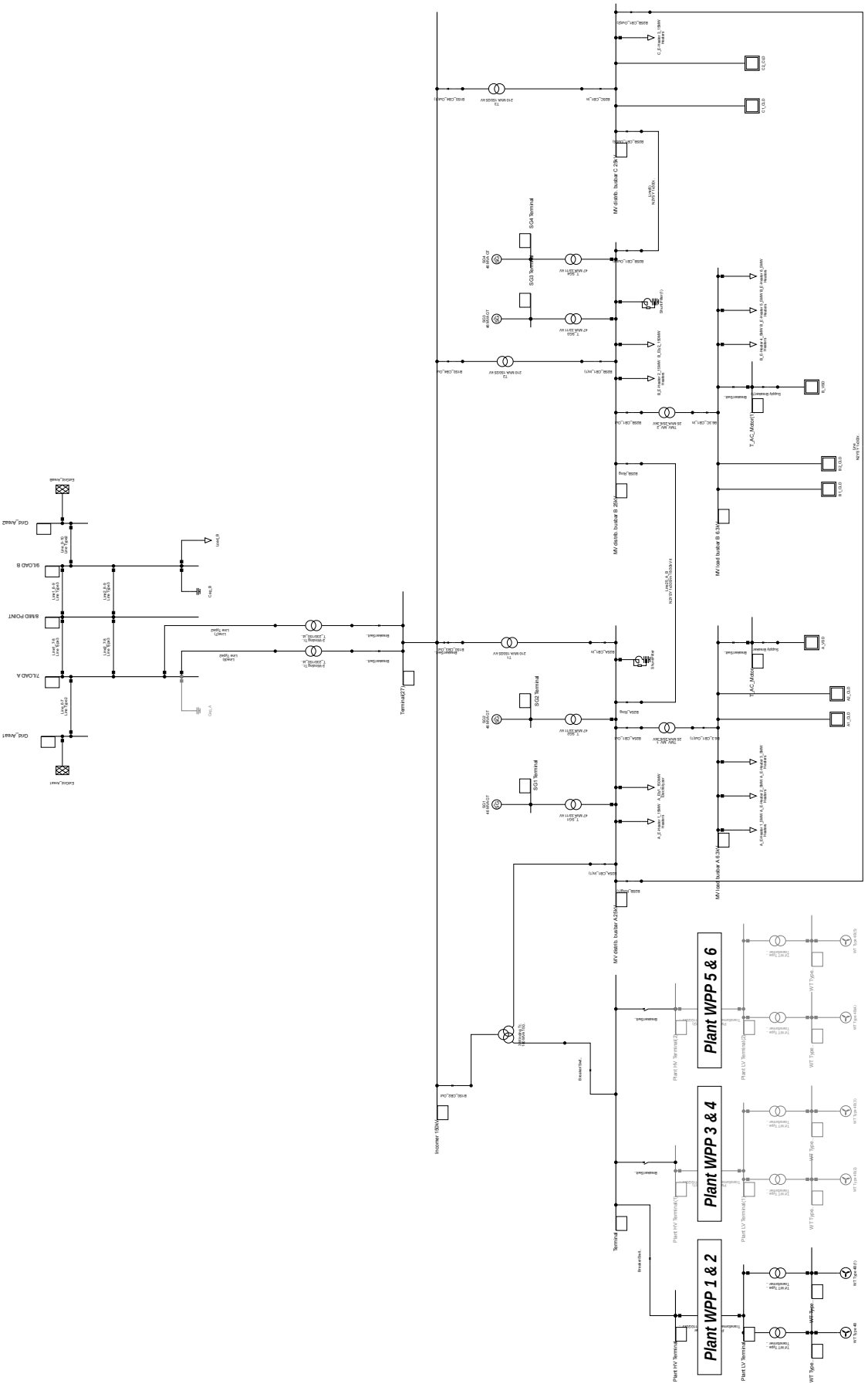

Figure B.1: Industrial hub network implemented in PowerFactory

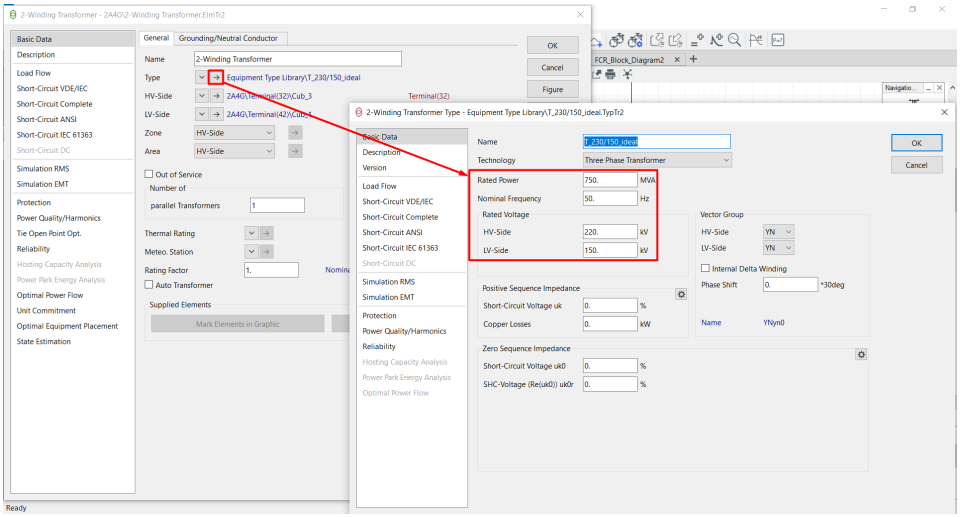

Figure B.2: Ideal transformer parameters

The parameters within the red boxes in Figure B.3 should be adjusted to modify the external grid representation.

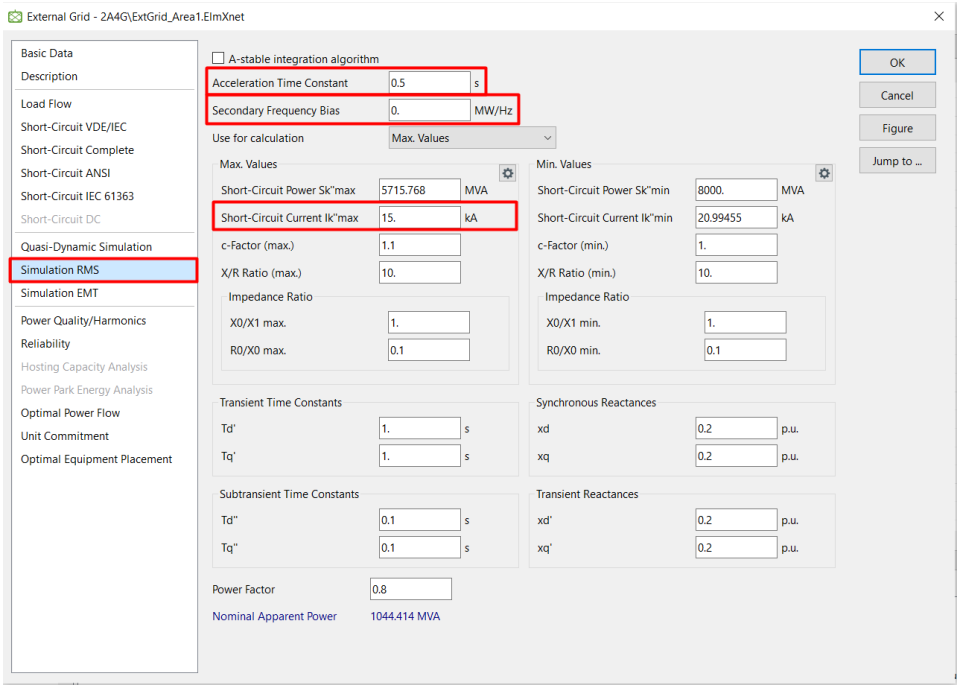

Figure B.3: External Grid parameters

For the SG, WPPs, VSDs, electrolyzer, and aggregated induction machines, composite frames containing the dynamic models and controllers are available in the data. In particular, the WECC composite load model includes a Python script that can be used to parameterize the aggregated load (Data Manager > WECC CMPLDW Configuration). By right-clicking and editing the file, the parameters can be tuned. The changes are only implemented when executing the script, as indicated in Figure B.4.

The tripping conditions are set on the DSL models pointed in Figure B.5.

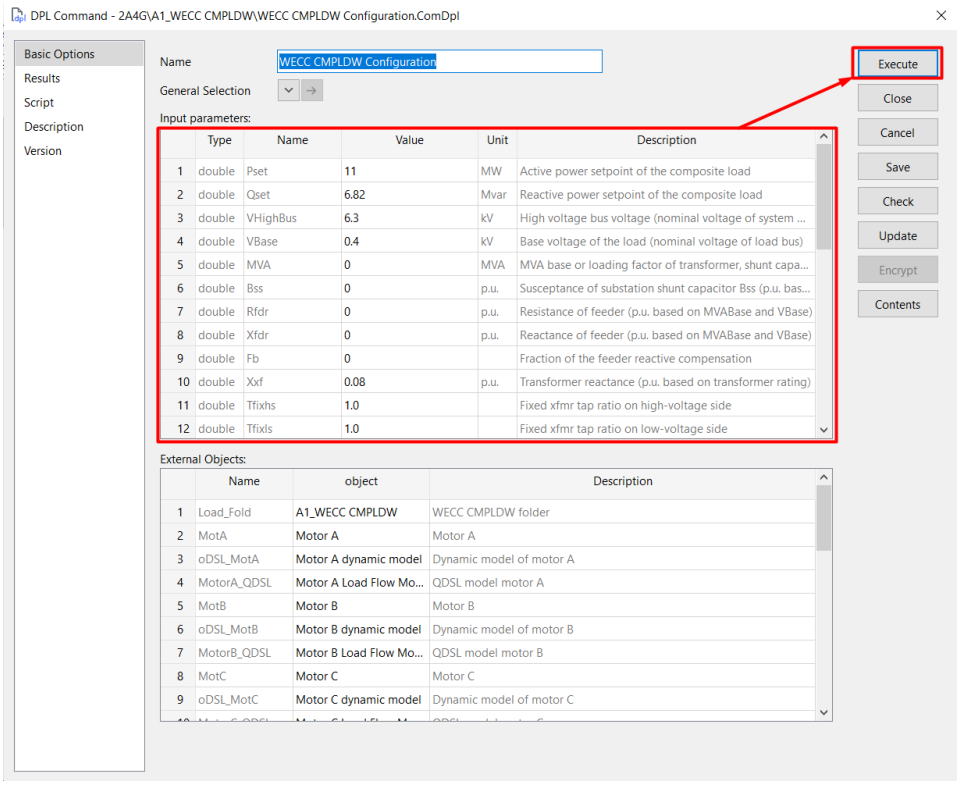

Figure B.4: WECC Composite model configuration

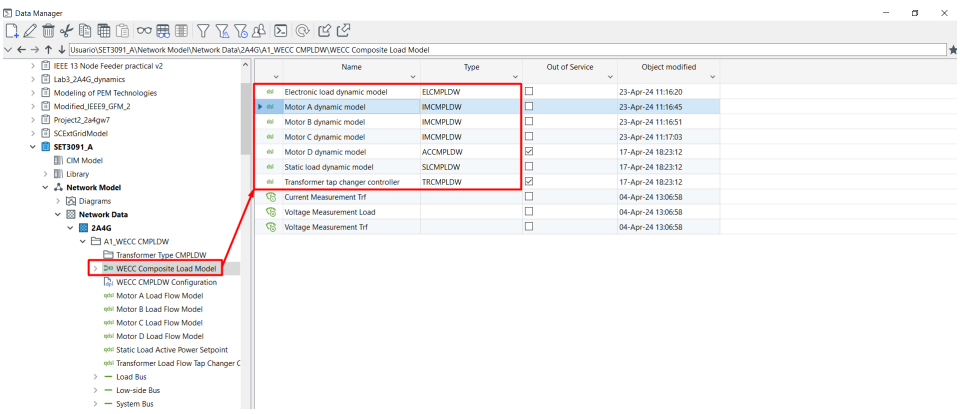

Figure B.5: WECC Composite model tripping settings

Similarly, the electrolyzer has a DSL model that implements the droop characteristic. The settings for such controller can be modified as shown in Figure B.6

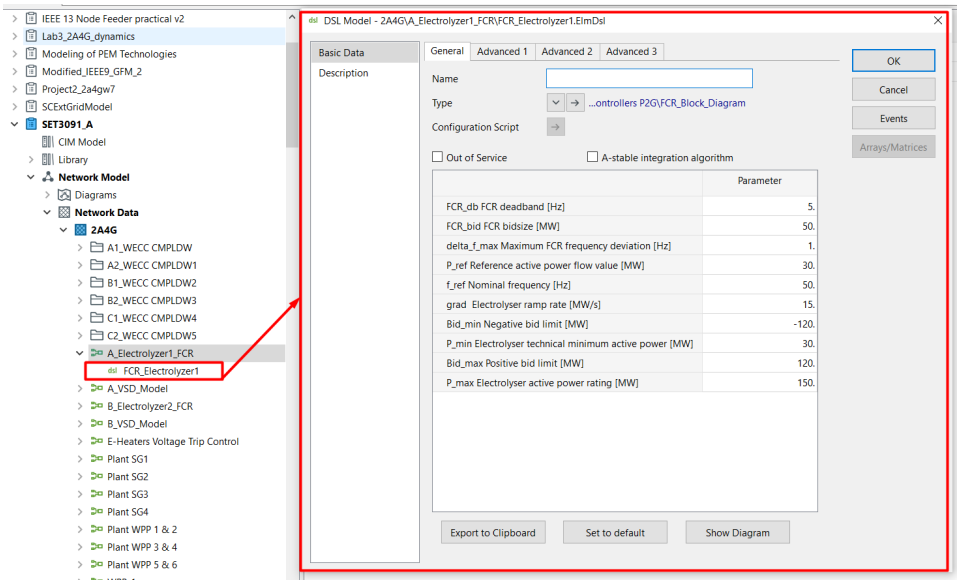

Figure B.6: Electrlyzer droop controller

To implement the synchronous condenser, the SG machine should be set to be a motor (as in Figure B.7). At the same time, the governor and power system stabilizer should be disabled (refer to Figure B.8). In addition, the exciter settings should be adapted accordingly. For the flywheel, the inertia constant should be tuned as shown in Figure B.9

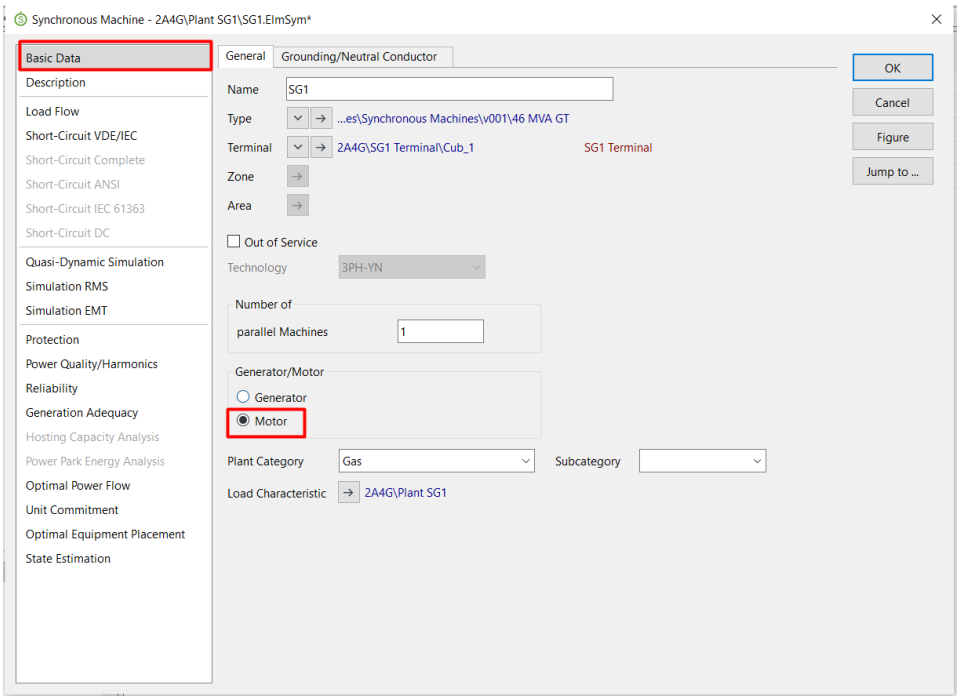

Figure B.7: Synchronous condenser

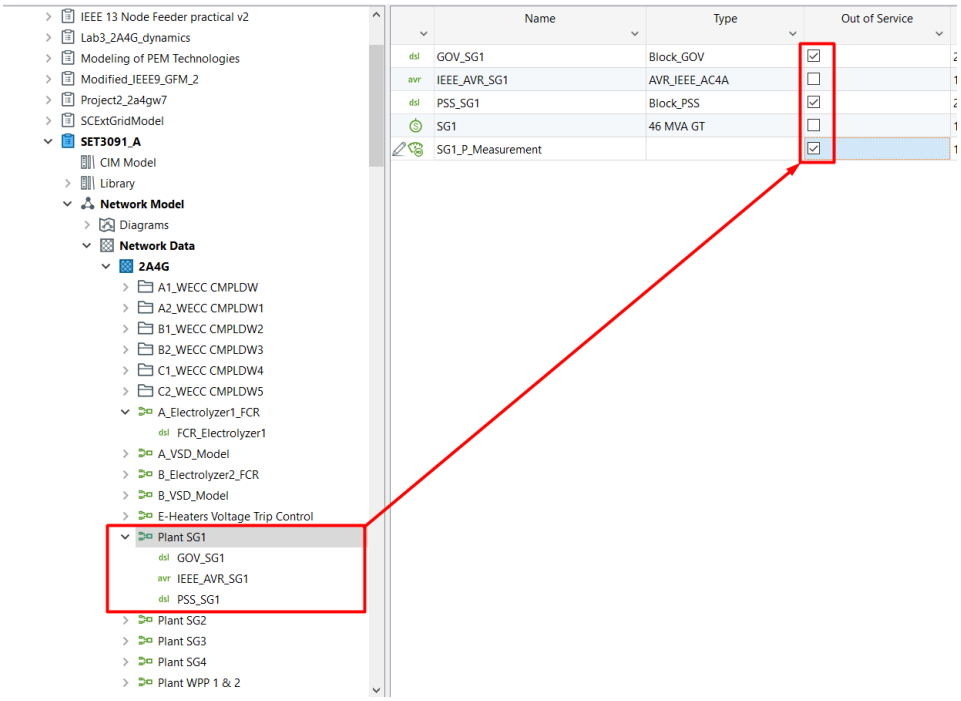

Figure B.8: Synchronous condenser controllers

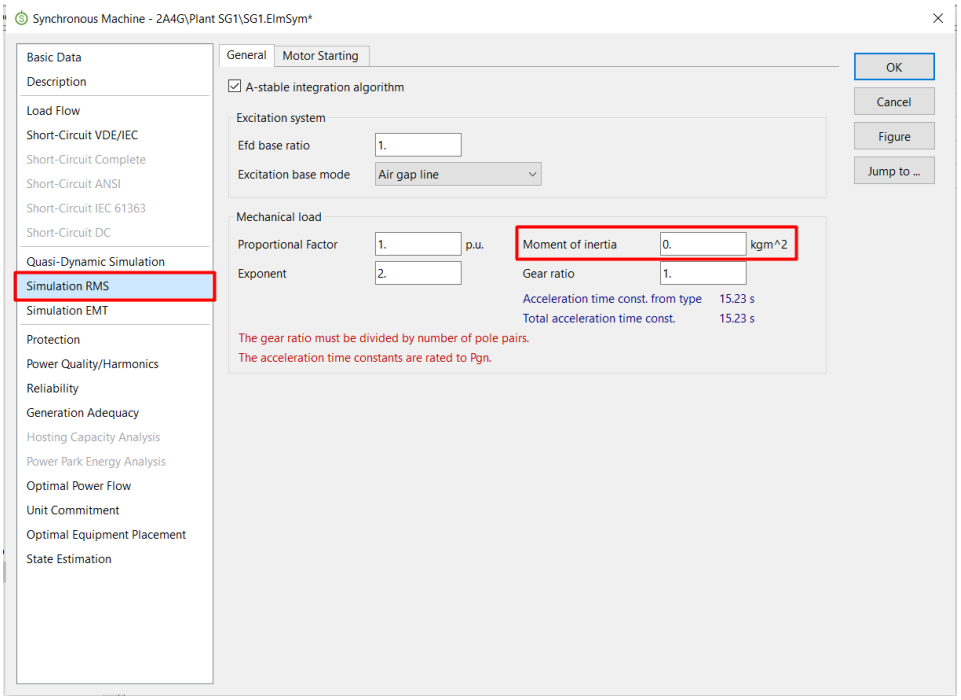

Figure B.9: Flywheel inertia settings